POLITECNICO DI TORINO
Repository ISTITUZIONALE

Measurement of D-0, D+, D+* and D-s(+) production in pp collisions at root s=5.02 TeV with ALICE

(Article begins on next page)

27 November 2024

THE EUROPEAN
PHYSICAL JOURNAL C

Regular Article - Experimental Physics

Measurement of D^0, D^+, D^{*+} and D_s^+ production in pp collisions at $\sqrt{s} = 5.02$ TeV with ALICE

ALICE Collaboration[*]

CERN, 1211 Geneva 23, Switzerland

Abstract The measurements of the production of prompt D^0, D^+, D^{*+}, and D_s^+ mesons in proton–proton (pp) collisions at $\sqrt{s} = 5.02$ TeV with the ALICE detector at the Large Hadron Collider (LHC) are reported. D mesons were reconstructed at mid-rapidity ($|y| < 0.5$) via their hadronic decay channels $D^0 \rightarrow K^-\pi^+$, $D^+ \rightarrow K^-\pi^+\pi^+$, $D^{*+} \rightarrow D^0\pi^+ \rightarrow K^-\pi^+\pi^+$, $D_s^+ \rightarrow \phi\pi^+ \rightarrow K^+K^-\pi^+$, and their charge conjugates. The production cross sections were measured in the transverse momentum interval $0 < p_T < 36$ GeV/c for D^0, $1 < p_T < 36$ GeV/c for D^+ and D^{*+}, and in $2 < p_T < 24$ GeV/c for D_s^+ mesons. Thanks to the higher integrated luminosity, an analysis in finer p_T bins with respect to the previous measurements at $\sqrt{s} = 7$ TeV was performed, allowing for a more detailed description of the cross-section p_T shape. The measured p_T-differential production cross sections are compared to the results at $\sqrt{s} = 7$ TeV and to four different perturbative QCD calculations. Its rapidity dependence is also tested combining the ALICE and LHCb measurements in pp collisions at $\sqrt{s} = 5.02$ TeV. This measurement will allow for a more accurate determination of the nuclear modification factor in p–Pb and Pb–Pb collisions performed at the same nucleon–nucleon centre-of-mass energy.

1 Introduction

The study of the production of hadrons containing heavy quarks, i.e. charm and beauty, in proton–proton (pp) collisions at LHC energies is a sensitive test of Quantum Chromodynamics (QCD) calculations with the factorisation approach. In this scheme, the transverse momentum (p_T) differential production cross sections of hadrons containing charm or beauty quarks are calculated as a convolution of three terms: (i) the parton distribution functions (PDFs) of the incoming protons, (ii) the partonic scattering cross section, calculated as a perturbative series in powers of the strong coupling constant α_s, and (iii) the fragmentation function, which parametrises the non-perturbative evolution of a heavy quark into a given species of heavy-flavour hadron. Factorisation is implemented in terms of the squared momentum transfer Q^2 (collinear factorisation) [1] or of the partonic transverse momentum k_T [2]. At LHC energies, calculations based on collinear factorisation are available in the general-mass variable-flavour-number scheme, GM-VFNS [3–6], and in the fixed order plus next-to-leading logarithms approach, FONLL [7,8], both of them having next-to-leading order (NLO) accuracy with all-order resummation of next-to-leading logarithms. Within the k_T-factorisation framework, heavy-flavour production cross-section calculations exist only at leading order (LO) approximation in α_s [2,9,10]. All these calculations describe within uncertainties the production cross sections of D and B mesons measured in pp and p$\bar{\text{p}}$ collisions in different kinematic regions at centre-of-mass energies from 0.2 to 13 TeV (see e.g. Ref. [11] and references therein). In the case of charm production, the uncertainties on the theoretical predictions, which are dominated by the choice of the scales of the perturbative calculation (e.g. the factorisation and renormalisation scales), are significantly larger than the uncertainties on the measured data points [12–23]. However, as pointed out in Ref. [24], in the ratios of cross sections at different LHC energies and in different rapidity intervals the uncertainty due to choice of the factorisation and renormalisation scales becomes subdominant with respect to the uncertainty on the PDFs, thus making the measurement sensitive to the gluon PDF at small Bjorken-x values. A precise measurement of the D-meson production cross sections down to $p_T = 0$ can therefore provide important constraints to perturbative QCD (pQCD) calculations and to low-x gluon PDFs. Furthermore, D-meson measurements in pp collisions represent an essential reference for the study of effects induced by cold and hot strongly-interacting matter in the case of proton–nucleus and nucleus–nucleus collisions (see e.g. the recent reviews [11,25,26]).

See Appendix A for the list of collaboration members

[a] e-mail: alice-publications@cern.ch

Springer

In this article, the measurements of the p_T-differential production cross sections of prompt D^0, D^+, D^{*+}, and D_s^+ mesons (as average of particles and anti-particles) in pp collisions at the centre-of-mass energy $\sqrt{s} = 5.02$ TeV are reported together with their ratios. The measurements are performed at mid-rapidity ($|y| < 0.5$) in the transverse momentum intervals $0 < p_T < 36$ GeV/c for D^0 mesons, $1 < p_T < 36$ GeV/c for D^+ and D^{*+} mesons, and $2 < p_T < 24$ GeV/c for D_s^+ mesons. The p_T-integrated D-meson production cross sections per unit of rapidity is also reported for each D-meson species. The ratios of the D^0, D^+, and D^{*+}-meson production cross sections measured at $\sqrt{s} = 7$ TeV [27] and $\sqrt{s} = 5.02$ TeV are presented as well, and compared to FONLL calculations. Finally, the ratios of D^0-meson production cross sections at mid- and forward rapidity are also reported, using the measurements done at forward rapidity by the LHCb collaboration in pp collisions at $\sqrt{s} = 5.02$ TeV [22].

2 Experimental apparatus and data sample

The ALICE experimental apparatus is composed of a set of detectors for particle reconstruction and identification at mid-rapidity, embedded in a large solenoidal magnet that provides a $B = 0.5$ T field parallel to the beams. It also includes a forward muon spectrometer and various forward and backward detectors for triggering and event characterisation. A complete description and an overview of their typical performance in pp, p–Pb, and Pb–Pb collisions is presented in Refs. [28,29].

The tracking and particle identification capabilities of the ALICE central barrel detectors were exploited to reconstruct the D-meson decay products at mid-rapidity. The Inner Tracking System (ITS), consisting of six cylindrical layers of silicon detectors, is used to track charged particles and to reconstruct primary and secondary vertices. The Time Projection Chamber (TPC) provides track reconstruction with up to 159 three-dimensional space points per track, as well as particle identification via the measurement of their specific ionisation energy loss dE/dx. The particle identification capabilities of the TPC are complemented by the Time-Of-Flight detector (TOF), which is used to measure the flight time of the charged particles from the interaction point. These detectors cover the pseudorapidity interval $|\eta| < 0.9$. The V0 detector, composed of two arrays of 32 scintillators each, covering the pseudorapidity ranges $-3.7 < \eta < -1.7$ and $2.8 < \eta < 5.1$, provides the minimum-bias (MB) trigger used to collect the data sample. In addition, the timing information of the two V0 arrays and the correlation between the number of hits and track segments in the two innermost layers of the ITS, consisting of Silicon Pixel Detectors (SPD), was used for an offline event selection, in order to

remove background due to the interaction between one of the beams and the residual gas present in the beam vacuum tube. In order to maintain a uniform acceptance in pseudorapidity, collision vertices were required to be within ± 10 cm from the centre of the detector in the beam-line direction. The pile-up events (less than 1%) were rejected by detecting multiple primary vertices using track segments defined with the SPD layers. After the aforementioned selections, the data sample used for the analysis consists of about 990 million MB events, corresponding to an integrated luminosity $L_{int} = (19.3 \pm 0.4)$ nb^{-1}, collected during the 2017 pp run at $\sqrt{s} = 5.02$ TeV.

3 Data analysis

3.1 Analysis with D-meson decay vertex reconstruction

The D mesons and their charge conjugates were reconstructed via the decay channels $D^0 \rightarrow K^-\pi^+$ (with branching ratio, BR $= 3.89 \pm 0.04\%$), $D^+ \rightarrow K^-\pi^+\pi^+$ (BR $= 8.98 \pm 0.28\%$), $D^{*+} \rightarrow D^0\pi^+ \rightarrow K^-\pi^+\pi^+$ (BR $= 2.63 \pm 0.03\%$), and $D_s^+ \rightarrow \phi\pi^+ \rightarrow K^+K^-\pi^+$ (BR $= 2.27 \pm 0.08\%$) [30]. The analysis was based on the reconstruction of decay vertices displaced from the interaction vertex, exploiting the separation of a few hundred μm induced by the weak decays of D^0, D^+, and D_s^+ mesons ($c\tau \simeq 123$, 312, and 150 μm, respectively [30]). The D^0, D^+, and D_s^+ candidates were built combining pairs or triplets of tracks with the proper charge, each with $|\eta| < 0.8$, $p_T > 0.3$ GeV/c, at least 70 associated TPC space points, χ^2/ndf < 2 in the TPC (where ndf is the number of degrees of freedom involved in the track fit procedure), and at least one hit in either of the two layers of the SPD. The D^{*+} candidates were defined by the combination of D^0 candidates with tracks reconstructed with at least two points in the ITS, including at least one in the SPD, and $p_T > 80$ MeV/c. As a consequence of these track selection criteria, the acceptance for D mesons decreases rapidly for $|y| > 0.5$ at low p_T and for $|y| > 0.8$ for $p_T > 5$ GeV/c. Therefore, only D-meson candidates within a fiducial acceptance region, $|y| < y_{fid}(p_T)$, were selected. The $y_{fid}(p_T)$ factor was defined as a second-order polynomial function, increasing from 0.5 to 0.8 in the transverse momentum range $0 < p_T < 5$ GeV/c, and a constant term, $y_{fid} = 0.8$, for $p_T > 5$ GeV/c.

In order to reduce the combinatorial background and to increase the signal-over-background ratio (S/B), geometrical selections on the D^0, D^+, and D_s^+-meson decay topology were applied. In the $D^{*+} \rightarrow D^0\pi^+$ case, the decay vertex cannot be resolved from the primary vertex and geometrical selections were applied on the secondary vertex topology of the produced D^0 mesons. The selection requirements, tuned to provide a large statistical significance for the sig-

nal and to keep the selection efficiency as high as possible, were mainly based on the displacement of the tracks from the primary vertex (d_0), the distance between the D-meson decay vertex and the primary vertex (decay length, L), and the pointing of the reconstructed D-meson momentum to the primary vertex. Additional selection criteria, already introduced in Refs. [27,31], were applied to D^+ and D_s^+ candidates. These selections reject both combinatorial background and D mesons from beauty-hadron decays (selection efficiency reduced by 50% at high p_T), denoted as "feed-down" in the following. For the D_s^+-candidate selection, one of the two pairs of opposite-sign tracks was required have a reconstructed K^+K^- invariant mass within ± 10 MeV/c^2 with respect to the PDG world average of the ϕ meson [30].

Further reduction of the combinatorial background was obtained by applying particle identification (PID) to the decay tracks, except for the soft-pion track coming from $D^{*+} \rightarrow D^0\pi^+$ decays. Pions and kaons were identified requiring compatibility with the respective particle hypothesis within three standard deviations (3σ) between the measured and the expected signals for both the TPC dE/dx and the time-of-flight. Tracks without TOF hits were identified using only the TPC information with a 3σ selection, except for the decay products of D_s^+ candidates with $p_T < 6$ GeV/c, for which a 2σ selection was needed to suppress the larger fraction of combinatorial background in this mode.

The D-meson raw yields, including both particles and antiparticles, were obtained from binned maximum likelihood fits to the invariant-mass (M) distributions of D^0, D^+, and D_s^+ candidates and to the mass difference $\Delta M = M(K\pi\pi) - M(K\pi)$ distributions of D^{*+} candidates, in the transverse-momentum intervals $0.5 < p_T < 36$ GeV/c for D^0 mesons, $1 < p_T < 36$ GeV/c for D^+ and D^{*+} mesons, and $2 < p_T < 24$ GeV/c for D_s^+ mesons. The signal extraction was performed in finer p_T bins with respect to the previous measurements at $\sqrt{s} = 7$ TeV [27], allowing for a more detailed description of the cross-section p_T shape. The fit function was composed of a Gaussian for the description of the signal and of an exponential term for the background of D^0, D^+, and D_s^+ candidates, and of a threshold function for D^{*+} candidates [27]. For the D^0 meson, the contribution of signal candidates present in the invariant-mass distribution with the wrong decay-particle mass assignment (reflections) was included in the fit. It was modelled based on the invariant-mass distributions of the reflected signal in the simulation, which were parametrised as the sum of two Gaussian functions. The contribution of reflections is about $2\% - 3\%$ of the raw signal depending on p_T. For the $M(KK\pi)$ distribution, an additional Gaussian was used to describe the signal of the decay $D^+ \rightarrow K^+K^-\pi^+$, with a branching ratio of $(9.51 \pm 0.34) \times 10^{-3}$ [30], present on the left side of the D_s^+-meson signal. Figure 1 shows the invariant mass (mass-difference) distributions together with the result of the

fits, in $1.5 < p_T < 2$ GeV/c, $16 < p_T < 24$ GeV/c, $7 < p_T < 7.5$ GeV/c, and $3 < p_T < 4$ GeV/c intervals for D^0, D^+, D^{*+}, and D_s^+ candidates, respectively. The statistical significance of the observed signals, $S/\sqrt{(S+B)}$, varies from 4 to 28, depending on the meson species and on the p_T interval. The S/B values obtained applying the selections described above are 0.01–1.85 for D^0, 0.5–2.2 for D^+, 0.3–4.2 for D^{*+}, and 0.3–2.2 for D_s^+ mesons, depending on p_T.

The p_T-differential cross section of prompt D mesons in each p_T interval was computed as:

$$\frac{\mathrm{d}^2\sigma^{\mathrm{D}}}{\mathrm{d}p_T\mathrm{d}y} = \frac{1}{c_{\Delta y}(p_T)\Delta p_T} \cdot \frac{1}{\mathrm{BR}}$$
$$\cdot \frac{\frac{1}{2} f_{\mathrm{prompt}}(p_T) \cdot N^{\mathrm{D}+\overline{\mathrm{D}},\mathrm{raw}}(p_T)\Big|_{|y|<y_{\mathrm{fid}}(p_T)}}{(\mathrm{Acc} \times \varepsilon)_{\mathrm{prompt}}(p_T)} \frac{1}{L_{\mathrm{int}}} . \quad (1)$$

The raw yield values (sum of particles and antiparticles, $N^{\mathrm{D}+\overline{\mathrm{D}},\mathrm{raw}}$) were divided by a factor of two and multiplied by the prompt fraction f_{prompt} to obtain the charged-averaged yields of prompt D mesons. Furthermore, they were divided by the acceptance-times-efficiency of prompt D mesons $(\mathrm{Acc} \times \varepsilon)_{\mathrm{prompt}}$, the BR of the decay channel, the width of the p_T interval (Δp_T), the correction factor for the rapidity coverage $c_{\Delta y}$, and the integrated luminosity $L_{\mathrm{int}} = N_{\mathrm{ev}}/\sigma_{\mathrm{MB}}$, where N_{ev} is the number of analysed events and $\sigma_{\mathrm{MB}} = (50.9 \pm 0.9)$ mb is the cross section for the MB trigger condition [32].

The $(\mathrm{Acc} \times \varepsilon)$ correction was obtained simulating pp collisions with the PYTHIA 6.4.25 event generator [33] (Perugia-11 tune [34]), and propagating the generated particles through the detector using GEANT3 [35]. Each simulated PYTHIA pp event contained a $c\bar{c}$ or $b\bar{b}$ pair, and D mesons were forced to decay into the hadronic channels of interest for the analysis. The luminous region distribution and the conditions of all the ALICE detectors in terms of active channels, gain, noise level and alignment, and their evolution with time during the data taking, were taken into account in the simulations.

Figure 2 shows the $(\mathrm{Acc} \times \varepsilon)$ as a function of p_T for prompt and feed-down D^0, D^+, D^{*+}, and D_s^+ mesons within the fiducial acceptance region. The average larger displacement from the primary vertex of beauty hadrons due to their long lifetime ($c\tau \approx 500$ μm [30]) results in a more efficient selection of feed-down D mesons compared to prompt D mesons in most of the p_T intervals.

The correction factor for the rapidity acceptance $c_{\Delta y}$ was computed with the PYTHIA 6.4.25 event generator with Perugia-11 tune. It was defined as the ratio between the generated D-meson yield in $\Delta y = 2\,y_{\mathrm{fid}}$, and that in $|y| < 0.5$. It was checked that calculations of the $c_{\Delta y}$ correction factor based on FONLL pQCD calculations [8] or on the assump-
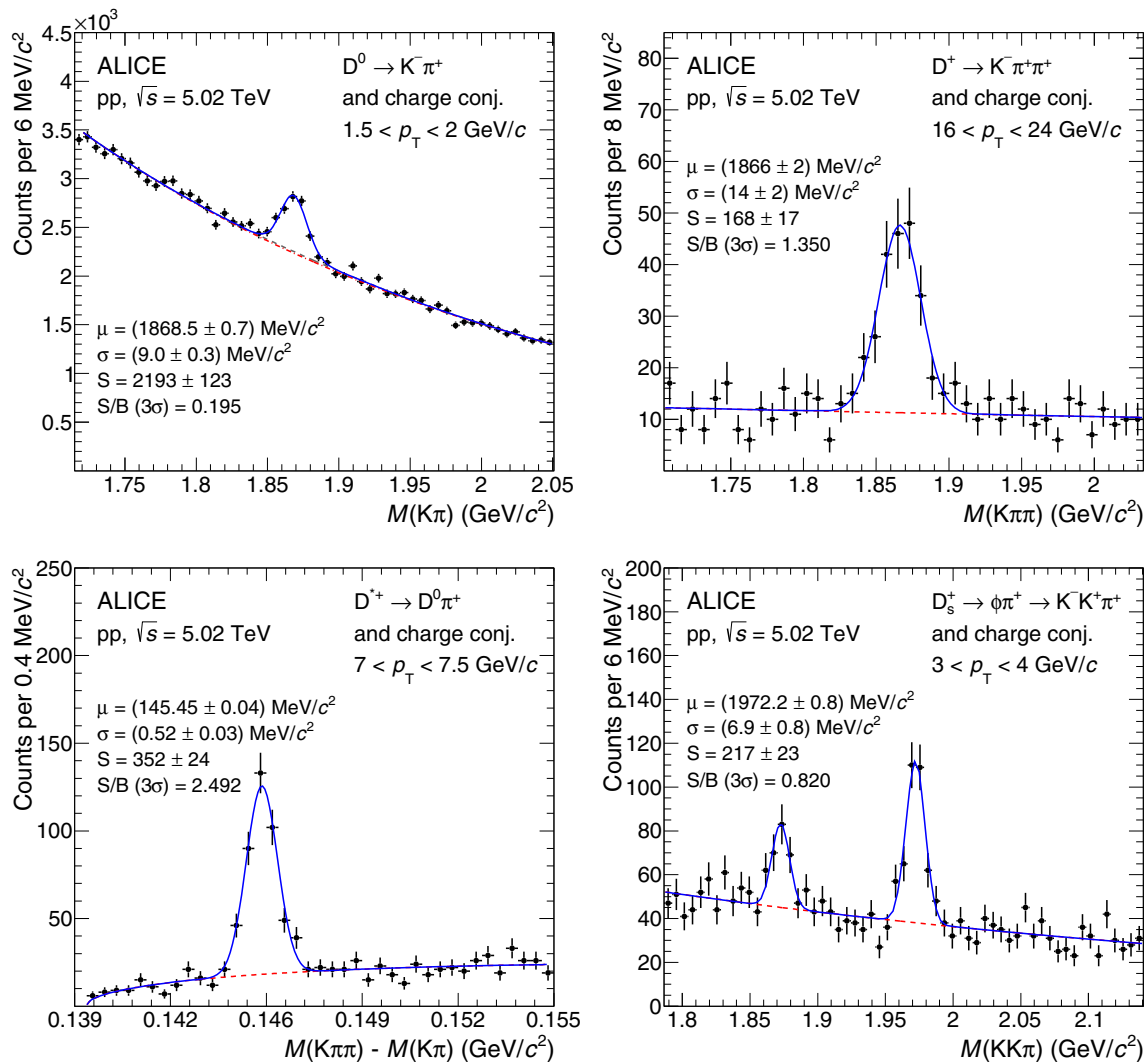
Fig. 1 Invariant-mass (mass-difference) distributions of D^0, D^+, D^{*+}, and D_s^+ candidates and charge conjugates in $1.5 < p_T < 2$ GeV/c, $16 < p_T < 24$ GeV/c, $7 < p_T < 7.5$ GeV/c, and $3 < p_T < 4$ GeV/c intervals, respectively. The blue solid lines show the total fit functions as described in the text and the red dashed lines are the combinatorial-background terms. In case of D^0, the grey dashed line represents the combinatorial background with the contribution of the reflections. The values of the mean (μ) and the width (σ) of the signal peak are reported together with the signal counts (S) and the signal over background ratio (S/B) in the mass interval ($\mu - 3\sigma$, $\mu + 3\sigma$). The reported uncertainties are only the statistical uncertainties from the fit

tion of uniform D-meson rapidity distribution in $|y| < y_{fid}$ would give the same result, because both in PYTHIA and in FONLL the D-meson yield is uniform within 1% in the range $|y| < 0.8$.

The f_{prompt} fraction was calculated similarly to previous measurements (see e.g. Refs. [27,31]) using the beauty-hadron production cross sections from FONLL calculations [7,36], the beauty hadron $\rightarrow$ D + X decay kinematics from the EvtGen package [37], and the efficiencies for feed-down D mesons reported in Fig. 2. The values of f_{prompt} range between 0.8 and 0.96 depending on D-meson species and p_T.

3.2 Analysis without D-meson decay vertex reconstruction

A different analysis method, not based on geometrical selections of the displaced decay-vertex topology, was developed for the two-body decay $D^0 \rightarrow K^-\pi^+$ (and its charge conjugate) in order to extend the measurement of the cross section down to $p_T = 0$ [19]. Indeed, the poor track impact parameter resolution at very low p_T and the small Lorentz boost limit the effectiveness of the selections based on the displaced decay-vertex topology. Furthermore, geometrical selections based on the displacement of the D^0-meson decay vertex tend to enhance the contribution of feed-down D mesons, increasing the related systematic uncertainty. This alternative analysis
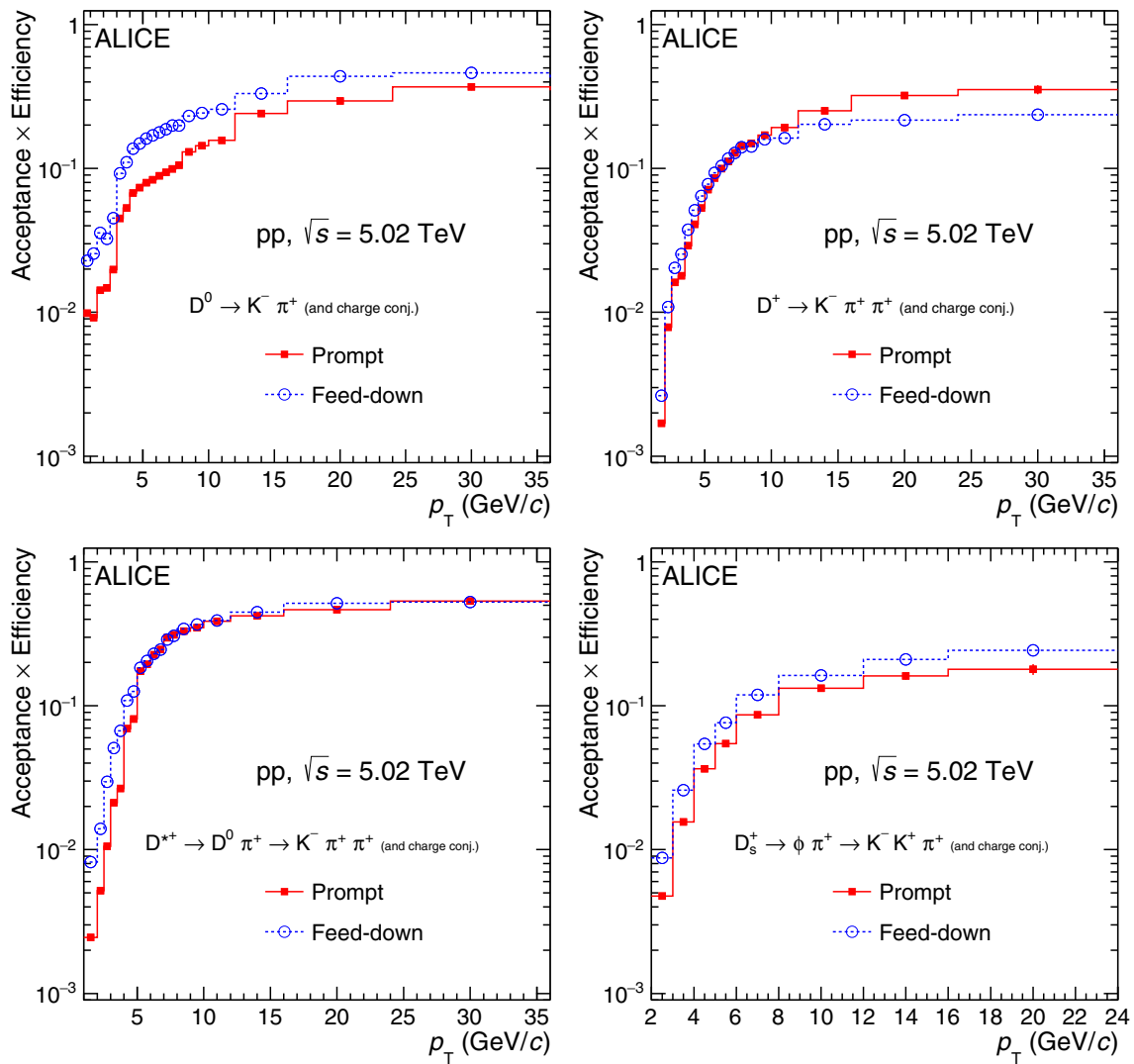
Fig. 2 Acceptance × efficiency for D^0, D^+, D^{*+}, and D_s^+ mesons, as a function of p_T. The efficiencies for prompt (solid lines) and feed-down (dotted lines) D mesons are shown
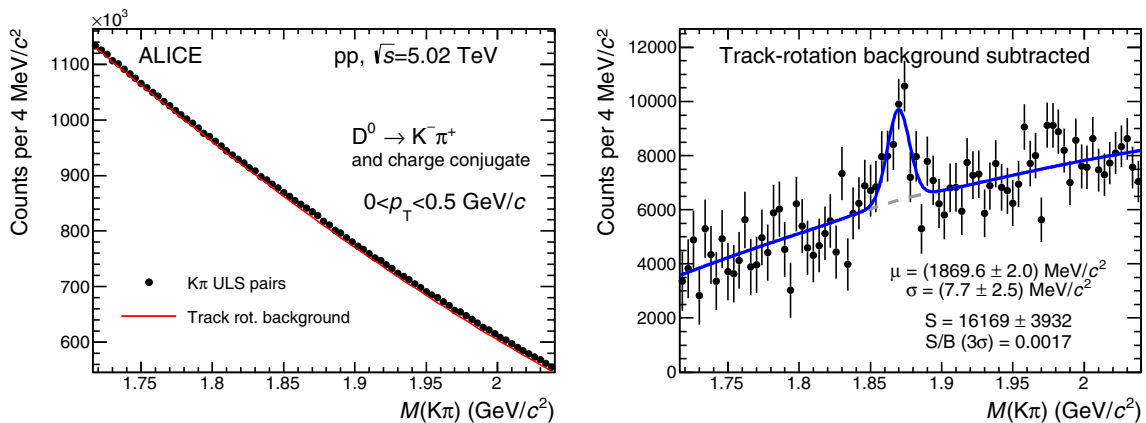
Fig. 3 Invariant-mass distributions of $D^0 \rightarrow K^-\pi^+$ candidates (and charge conjugates) for $0 < p_T < 0.5$ GeV/c. The left panel displays the invariant-mass distribution of all opposite-sign $K\pi$ pairs (or unlike sign, ULS in the legend) together with the background distribution estimated with the track-rotation technique. The right panel shows the invariant-

mass distributions after subtraction of the background from the track-rotation technique. The blue solid line shows the total fit function as described in the text and the grey dashed line is the residual background after the subtraction of the background from the track-rotation technique

technique is mainly based on particle identification and on the estimation and subtraction of the combinatorial background.

The D^0 candidates were formed combining pairs of kaons and pions tracks with opposite charge sign, $|\eta| < 0.8$, and $p_T > 0.3$ GeV/c. Track selection and pion and kaon identification were performed with the same strategy used in the analysis with decay-vertex reconstruction described in Sect. 3.1. The resulting D^0 and $\overline{D^0}$ candidates were selected by applying the same fiducial acceptance selection $|y| < y_{fid}(p_T)$ adopted for the analysis with decay-vertex reconstruction. The invariant-mass distribution of Kπ pairs was obtained in fourteen transverse momentum intervals, in the range $0 < p_T < 12$ GeV/c. The background distribution was estimated with the track-rotation technique. For each D^0 (and $\overline{D^0}$) candidate, up to 19 combinatorial-background-like candidates were created by rotating the kaon track by different angles in the range between $\frac{\pi}{10}$ and $\frac{19\pi}{10}$ radians in azimuth. The left hand panel of Fig. 3 shows the invariant-mass distribution of opposite-sign Kπ pairs together with that of the background estimated with the track-rotation technique in the interval $0 < p_T < 0.5$ GeV/c.

After subtracting the background distribution from the opposite-sign Kπ invariant-mass distribution, the D^0-meson raw signal (sum of particle and antiparticle contributions) was extracted from the resulting distribution via a fit to the background-subtracted invariant-mass distribution, as reported in Fig. 3 (right panel) for the interval $0 < p_T < 0.5$ GeV/c. In the fit function, the signal was modelled with a Gaussian term, while the residual background with second-order polynomial function. The statistical significance of the signal extracted in $0 < p_T < 0.5$ GeV/c ($0.5 < p_T < 1$ GeV/c) is $S/\sqrt{S+B} = 5.2$ (8.0).

The (Acc $\times \varepsilon$) correction factors of prompt and feed-down D^0 mesons were determined from the same Monte Carlo simulations as those used for the analyses with decay-vertex reconstruction. The (Acc $\times \varepsilon$) obtained with the two different analyses are compared in Fig. 4. For the analysis that does not exploit the selections on the D^0-meson decay vertex, the efficiency is higher by a factor of about 30 (3) at low (high) p_T and almost independent of p_T. The mild increase with the increasing p_T is mainly determined by the geometrical acceptance of the detector. Unlike in the analysis with decay-vertex reconstruction, the efficiency is the same for prompt D^0 and for feed-down D^0, as expected when no selection is made on the displacement of the D^0-meson decay vertex from the interaction point.

The prompt fraction to the D^0-meson raw yield, f_{prompt}, was estimated with the same FONLL-based approach used for the analysis with decay-vertex. The resulting f_{prompt} values decrease with increasing p_T, from a value of about 0.95 for $p_T < 4$ GeV/c to about 0.90 in the interval $8 < p_T < 12$ GeV/c and are larger compared to the analysis with decay-vertex reconstruction, due to the fact that the
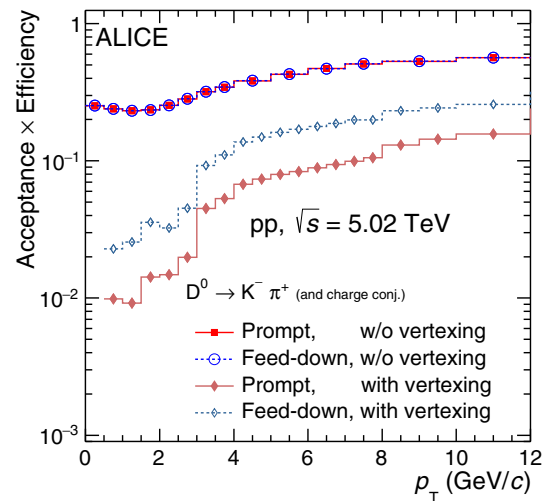
Fig. 4 Product of acceptance and efficiency of $D^0 \rightarrow K^-\pi^+$ (and charge conjugates)

feed-down component is not enhanced by the topological selection criteria.

3.3 Measurement of the fraction of prompt D mesons

In order to cross-check the values obtained with the FONLL-based method of Sect. 3.1, the fractions of prompt D^0 and D_s^+ mesons in the raw yields, f_{prompt}, were measured exploiting the different shapes for the distributions of the transverse-plane impact parameter to the primary vertex (d_0) of prompt and feed-down D mesons. The prompt fraction was estimated via an unbinned maximum-likelihood fit of the d_0 distribution of D^0 and D_s^+ candidates with invariant mass $|M - M_D| < 2\sigma$ (where σ is the standard deviation of the Gaussian function describing the D-meson signal in the invariant-mass fits), using the fit function

$$F(d_0) = S \cdot \left[(1 - f_{prompt}) F^{feed\text{-}down}(d_0) \right.$$
$$\left. + f_{prompt} F^{prompt}(d_0) \right] + B \cdot F^{backgr}(d_0) . \quad (2)$$

In this function, S and B are the signal raw yield and background in the selected invariant-mass range, fixed to the values obtained from the invariant-mass fit; $F^{prompt}(d_0)$, $F^{feed\text{-}down}(d_0)$, and $F^{backgr}(d_0)$ are the functions describing the impact-parameter distributions of prompt and feed-down D mesons and background, respectively. The function F^{prompt} is a detector resolution term modelled with a Gaussian and a symmetric exponential term. The function $F^{feed\text{-}down}$ is the convolution of a sum of two symmetric exponential functions ($F^{feed\text{-}down}_{true}$), which describe the intrinsic impact-parameter distribution of secondary D mesons from beauty-hadron decays, and the detector resolution term (F^{prompt}). All the parameters of the F^{prompt} and $F^{feed\text{-}down}_{true}$ functions were fixed in the data fit to the values obtained

by fitting the distributions from Monte Carlo simulations, except for the Gaussian width of the detector-resolution term, which was kept free in order to compensate a possible discrepancy between the impact-parameter resolution in the data and in the simulation. The distribution describing the combinatorial background was parameterised with a function composed of a Gaussian and symmetric exponential term (F^{backgr}). The parameters were fixed to those obtained by fitting the impact-parameter distribution of background candidates in the side bands of the signal peak in the invariant-mass distributions. Figure 5 (left) shows examples of fits to the impact-parameter distributions of D^0 and D_s^+ mesons in the transverse-momentum intervals $3 < p_T < 4$ GeV/c and $5 < p_T < 6$ GeV/c, respectively. For this study, wider p_T intervals were adopted compared to the analysis, due to the poor quality of the fit when reducing the sample. The D^0 candidates used in the impact-parameter fit were selected with the same criteria described in Sect. 3.1. For the D_s^+ mesons, the impact-parameter selection, used to extract the raw yield from the invariant-mass distribution, was not applied for this study. In this case, the prompt fraction, f_{prompt}, was obtained by integrating the functions obtained from the fit in the restricted impact-parameter range used in the analysis.

The prompt fraction measured with the fits to the impact-parameter distributions of D-meson candidates has three main sources of systematic uncertainty, namely (i) the assumption on the shape of the impact-parameter distribution for each contribution (prompt D mesons, feed-down D mesons, and combinatorial background); (ii) the uncertainty on the signal and background yields extracted from the invariant-mass fits; and (iii) the consistency of the procedure, evaluated with a Monte Carlo closure test. These uncertainties were estimated with the procedures described in Ref. [19]. The total systematic uncertainty on f_{prompt} with the data-driven approach ranges, depending on p_T, are between 1 and 9% for the D^0 meson, and between 4 and 17% for the D_s^+ meson.

The prompt fractions in the raw yields of D^0 and D_s^+ mesons measured with the data-driven method are compared to those calculated with the FONLL-based approach in the right panels of Fig. 5 and found to be compatible within uncertainties. For the interval $24 < p_T < 36$ GeV/c ($16 < p_T < 24$ GeV/c), given the poor precision of the impact-parameter fit, it was not possible to determine the data-driven prompt fraction for the D^0 (D_s^+) meson.

4 Systematic uncertainties

Systematic uncertainties on the D-meson cross sections were estimated considering the following sources: (i) extraction of the raw yield from the invariant-mass distributions; (ii) track reconstruction efficiency; (iii) D-meson selection efficiency;

(iv) PID efficiency; (v) the shape of the p_T spectrum generated for D mesons in the simulation; (vi) subtraction of the feed-down from beauty-hadron decays. In addition, the uncertainties on the branching ratios and on the integrated luminosity were considered. A summary of the systematic uncertainties is reported in Table 1 for different p_T intervals.

The systematic uncertainties on the raw yield extraction were evaluated by repeating the fits several hundred times varying the fit interval and the functional form of the background fit function. The same strategy was performed using a bin-counting method, in which the signal yield was obtained by integrating the invariant-mass distribution after subtracting the background, estimated from a fit to the side-bands only. The systematic uncertainty was defined as the RMS of the distribution of the signal yields obtained from all these variations and ranges between 1 and 9% depending on the D-meson species and p_T interval. This includes for the D^0 mesons a contribution of about 1% obtained by varying the ratio of the integral of the reflections to the integral of the signal and the shape of the templates used in the invariant-mass fits. For the background estimation of the D^0-meson analysis without decay-vertex reconstruction with the track-rotation technique, different configurations of the rotation angle were used. In addition, three alternative approaches were tested to estimate the background distribution: like-sign (LS) pairs, event mixing, and side-band fit [19]. The raw yield values obtained subtracting these alternative background distributions were found to be consistent with those from the default configuration of the track-rotation method within the uncertainty estimated by varying the fit conditions and therefore no additional systematic uncertainty was assigned.

The systematic uncertainty on the track reconstruction efficiency has two different contributions. The first one is estimated by varying the track-quality selection criteria and the second one is estimated by comparing the probability to match the tracks from the TPC to the ITS hits in data and simulation (matching efficiency). To obtain the matching efficiency, the abundances of primary and secondary particles in data were estimated via template fits to the track impact-parameter distributions, where the relative abundances in the simulation were weighted to match those in data [27,38]. The estimated uncertainty, a quadratic sum of the two contributions, depends on the D-meson p_T and it ranges from 3 to 5% for the two-body decay of D^0 mesons and from 3.5 to 7% for the three-body decays of D^+, D^{*+}, and D_s^+ mesons.

The systematic uncertainty on the D-meson selection efficiency originates from imperfections in the simulation of the D-meson decay kinematics and topology and of the resolutions and alignments of detectors in the simulation. For the analyses with decay-vertex reconstruction, the systematic uncertainty was estimated by repeating the analysis with different sets of selection criteria, resulting in a significant modification of the efficiencies, raw yield, and background
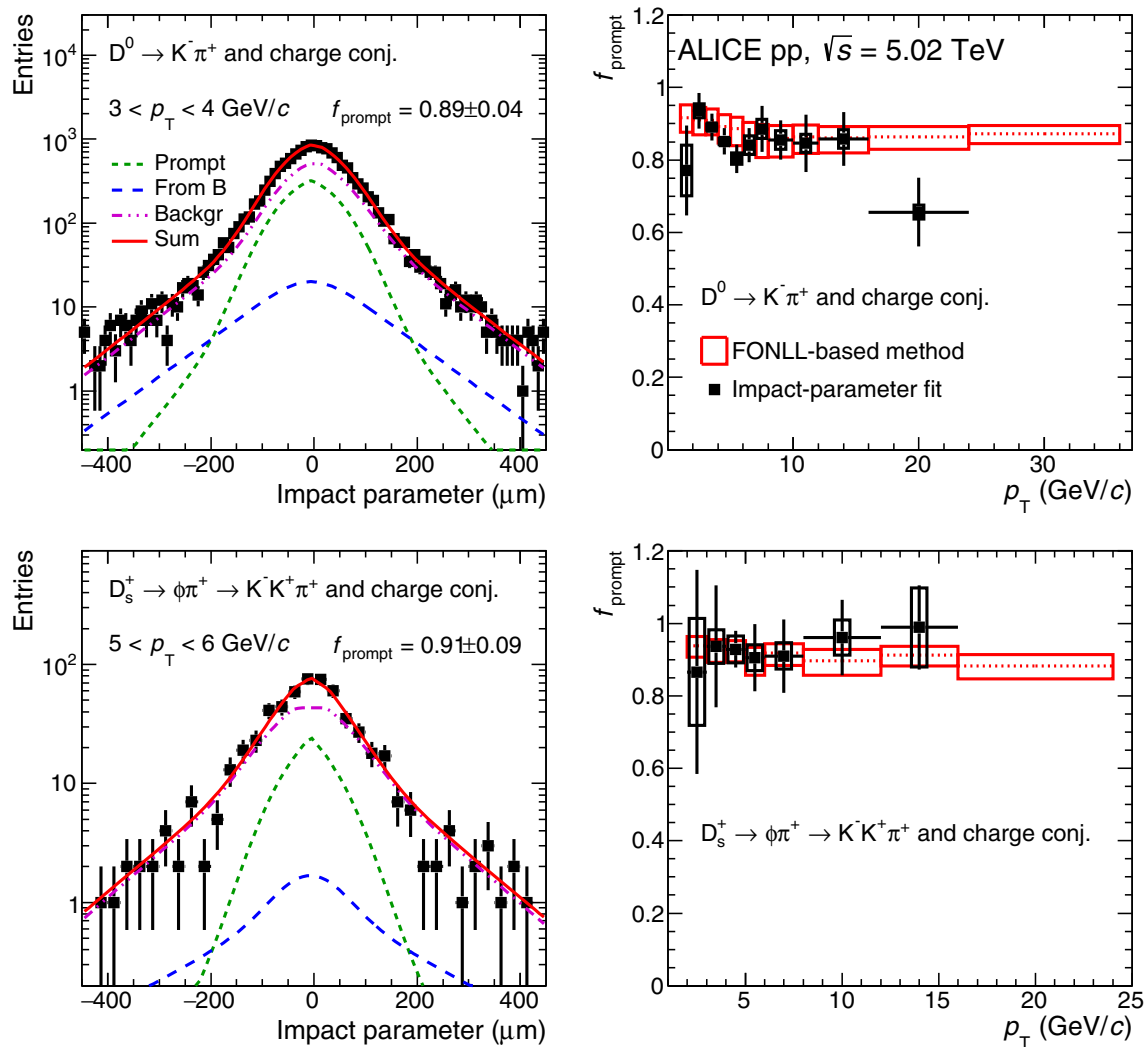
Fig. 5 Left: examples of fits to the impact-parameter distributions of D^0 and D_s^+ candidates. The curves show the fit functions describing the prompt, feed-down, and background contributions, as well as their sum, as described in the text. Right: fraction of prompt D^0 and D_s^+-mesons raw yield as a function of p_T compared to the values obtained with the FONLL-based approach. The results from the data-driven method are shown as square markers with the error bars (boxes) representing the statistical (systematic) uncertainty. The central values of f_{prompt} from the FONLL-based approach are shown by the dashed line and their uncertainty by the red boxes

values. The systematic uncertainties are largest at low p_T (up to 5%), where the efficiencies are low and vary steeply with p_T, because of the tighter geometrical selections. For the D_s^+ meson, for which more stringent selection criteria were used, slightly larger uncertainties were estimated, ranging from 5% at high p_T to 8% at low p_T. In the case of the D^0-meson analysis without decay-vertex reconstruction, the stability of the corrected yield was tested against variations of the single-track p_T selection and no systematic effect was observed.

To estimate the uncertainty on the PID selection efficiency, the analysis was repeated without PID selection for the three non-strange D-meson species and D_s^+ mesons with $p_T > 6$ GeV/c. The resulting cross sections were found to be compatible with those obtained with the PID selection and therefore no systematic uncertainty was assigned. For D_s^+

mesons with $p_T < 6$ GeV/c and the D^0-meson analysis without decay-vertex reconstruction, an analysis without applying PID selections could not be performed due to the insufficient statistical significance of the signal. The systematic uncertainty for low-p_T D_s^+ mesons was therefore estimated by comparing the pion and kaon PID selection efficiencies in the data and in the simulation and combining the observed differences using the D_s^+-meson decay kinematics [31]. A 3% systematic uncertainty was assigned for $4 < p_T < 6$ GeV/c, and 2.5% for $p_T < 4$ GeV/c. For the D^0-meson analysis without decay-vertex reconstruction, compatible cross sections were obtained when using more stringent PID criteria. Based on this result and on the fact that the PID selections are the same as used in the analysis with decay-vertex reconstruction, no uncertainty due to PID was assigned.

Table 1 Summary of relative systematic uncertainties on D^0, D^+, D^{*+}, and D_s^+ measurements in different p_T intervals

p_T (GeV/c)	D^0			D^+		D^{*+}		D_s^+	
	0–0.5	2–2.5	10–12	2–2.5	10–12	2–2.5	10–12	2–3	8–12
Signal yield	9%	3%	2%	3%	3%	3%	1%	7%	3%
Tracking efficiency	3%	4%	5%	4.5%	7%	4%	5%	4.5%	7%
Selection efficiency	0	5%	3%	4%	3%	5%	1%	8%	5%
PID efficiency	0	0	0	0	0	0	0	2.5%	0
p_T shape in MC	0	0	0	1%	0	1%	0	1%	0
Feed-down	$^{+1.1}_{-1.3}$%	$^{+3.6}_{-4.3}$%	$^{+3.8}_{-5.3}$%	$^{+2.4}_{-2.8}$%	$^{+2.3}_{-3.1}$%	$^{+3.0}_{-3.5}$%	$^{+1.8}_{-2.5}$%	$^{+2.8}_{-3.3}$%	$^{+3.4}_{-4.5}$%
Branching ratio	1.0%			3.1%		1.3%		3.5%	
Luminosity	2.1%			2.1%		2.1%		2.1%	

The systematic uncertainty due to the generated D-meson p_T shape was estimated by using FONLL as an alternative generator with respect to PYTHIA to simulate the D-meson p_T distribution [15], and was found to be 0–5% for $p_T <$ 3 GeV/c and negligible at higher p_T. The p_T shape of both considered distributions were found to be compatible with the measured one within uncertainties. Finally, the systematic uncertainty on the subtraction of feed-down from beauty-hadron decays (i.e. the calculation of the f_{prompt} fraction) was estimated by varying the FONLL parameters (b-quark mass, factorisation, and renormalisation scales) as prescribed in Ref. [8]. It ranges between $^{+1.0}_{-1.2}$% and $^{+4.4}_{-6.3}$% depending on the D-meson species and p_T interval.

The contributions of these different sources of uncertainties were summed in quadrature to obtain the total systematic uncertainty in each p_T interval, which varies from 6.5 to 10.0%, 6.5 to 10.5%, 5.4 to 11.3%, and 8.7 to 12.1% for the D^0, D^+, D^{*+}, and D_s^+ mesons, respectively. The systematic uncertainty on PID, tracking, and selection efficiencies are mainly correlated among the different p_T intervals, while the raw-yield extraction uncertainty is mostly uncorrelated. The p_T-differential cross sections have an additional global normalisation uncertainty due to the uncertainties on the integrated luminosity [32] and on the branching ratios of the considered D-meson decays [30].

5 Results

5.1 Transverse momentum-differential cross sections

The p_T-differential production cross section for prompt D^0 mesons in $|y| < 0.5$ in pp collisions at $\sqrt{s} = 5.02$ TeV was obtained from the analyses with and without decay-vertex reconstruction. The two results are compared in Fig. 6 with the inset showing their ratio in the common p_T range. In all the figures in this section, the vertical error bars represent the statistical uncertainties and the systematic uncertainties are
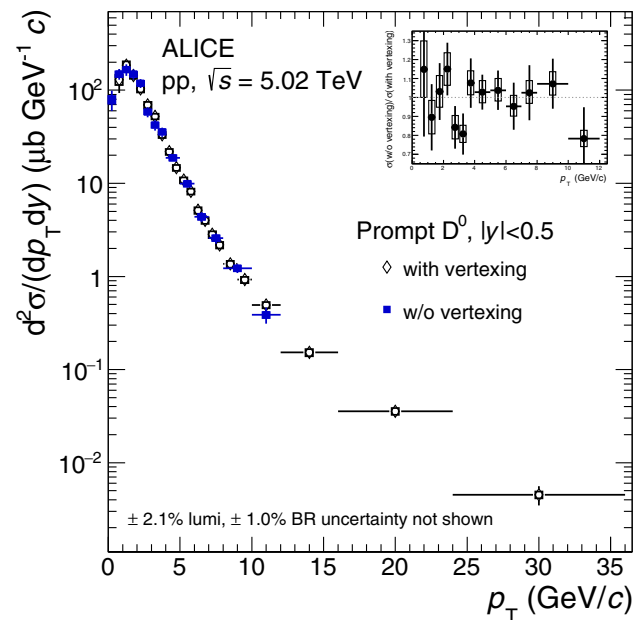
Fig. 6 Prompt D^0-meson p_T-differential production cross section in $|y| < 0.5$ in pp collisions at $\sqrt{s} = 5.02$ TeV measured with and without decay-vertex reconstruction. The inset shows the ratio of the measurements in their common p_T range. The vertical error bars and the empty boxes represent the statistical and systematic uncertainties, respectively

depicted as boxes around the data points. In each p_T interval the symbols are positioned horizontally at the center of the bin and the horizontal bars represents the width of the p_T interval. The two results for prompt D^0-meson cross section are found to be consistent within statistical uncertainties, which are independent between the two measurements because of their very different signal-to-background ratios and efficiencies. The most precise measurement of the prompt D^0-meson production cross section is obtained using the results of the analysis without decay-vertex reconstruction in the interval $0 < p_T < 1$ GeV/c and those of the analysis with decay-vertex reconstruction for $p_T > 1$ GeV/c.

The p_T-differential cross sections for prompt D^0, D^+, D^{*+}, and D_s^+-meson production in $|y| < 0.5$ are depicted
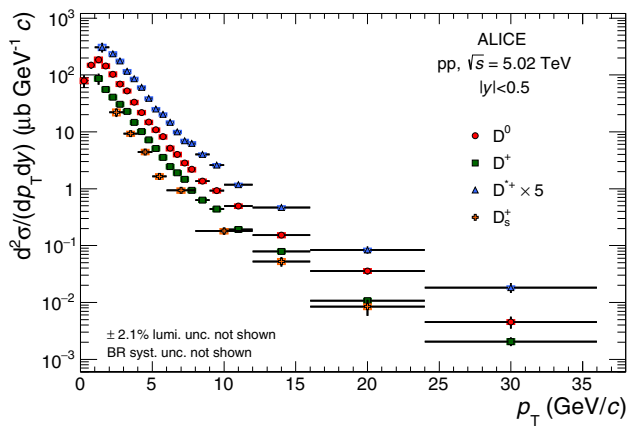
Fig. 7 p_T-differential production cross section of prompt D^0, D^+, D^{*+}, and D_s^+ mesons in pp collisions at $\sqrt{s}$ = 5.02 TeV. Statistical uncertainties (bars) and systematic uncertainties (boxes) are shown. For the D^0 meson, the results in $0 < p_T < 1$ GeV/c are obtained from the analysis without decay-vertex reconstruction, while those in $1 < p_T < 36$ GeV/c are taken from the analysis with decay-vertex reconstruction. The D^{*+}-meson cross section is scaled by a factor of 5 for better visibility

in Fig. 7. The prompt D^0-meson p_T-differential cross section is compatible with the one measured by the CMS collaboration at the same centre-of-mass energy in $|y| < 1$ and $2 < p_T < 100$ GeV/c [20].

In Figs. 8, 9, 10, and 11 the measured prompt D^0, D^+, D^{*+}, and D_s^+-meson p_T-differential cross sections are compared with results of pQCD calculations performed with different schemes: FONLL [7,8] (not available for the D_s^+ meson), two calculations using the GM-VNFS framework with different prescriptions to regulate the divergences at small transverse momentum, dubbed as GM-VFNS(mod-$\mu_{R,F}$) [39,40] and GM-VFNS(SACOT-m_T) [6], and a calculation based on k_T-factorisation [41]. The GM-VFNS(mod-$\mu_{R,F}$) calculations were performed with a different choice of the factorisation and renormalisation scales μ_F and μ_R with respect to the GM-VFNS predictions of Ref. [5] that were compared in Ref. [27] to the cross sections measured at $\sqrt{s} = 7$ TeV. With this modification of QCD scale, the calculations could be extended to lower p_T. In GM-VFNS(SACOT-m_T), the divergences of the heavy-quark PDFs and light-parton fragmentation functions at low p_T are regulated by the heavy-quark mass, thus allowing the calculation of the D-meson cross section down to $p_T = 0$. Note also that the authors of the k_T-factorisation calculations changed the treatment of the running strong coupling constant α_S and the gluon distributions [41], with respect to the predictions shown in Ref. [27]. In GM-VFNS(mod-$\mu_{R,F}$) the value of charm mass is set to 1.3 GeV/c^2, while in FONLL, GM-VFNS(SACOT-m_T) and k_T-factorisation predictions the mass is set to 1.5 GeV/c^2. The four frameworks utilise different sets of PDFs (CTEQ6.6 [42], CTEQ14 [43], NNPDF3.1 [44] and MMHT2014 [45] for FONLL, GM-VFNS(mod-$\mu_{R,F}$), GM-

VFNS(SACOT-m_T) and k_T-factorisation, respectively) and different fragmentation functions. The theoretical uncertainties are estimated by varying the factorisation and renormalisation scales in FONLL, GM-VFNS(SACOT-m_T) and k_T-factorisation, while only the renormalisation scale μ_R is varied in GM-VFNS(mod-$\mu_{R,F}$). In FONLL and k_T-factorisation calculations the charm-quark mass is also varied. The uncertainties on the PDFs are included in the GM-VFNS(SACOT-m_T) and FONLL predictions. The theoretical calculations are performed in the same p_T intervals as the measurements, except for the first bin of the D^0 prediction with GM-VFNS(mod-$\mu_{R,F}$) that starts from 0.1 GeV/c. The results of these calculations are shown as filled boxes spanning the theoretical uncertainties and a solid line representing the values obtained with the central values of the pQCD parameters.

The measured cross sections of non-strange D mesons are described within uncertainties by FONLL and the two GM-VFNS calculations. The data lie systematically on the upper edge of the uncertainty band of the FONLL predictions. For the two calculations in the GM-VFNS framework, the central values of the predictions tend to underestimate the data at low and intermediate p_T and to overestimate them at high p_T. The k_T-factorisation predictions describe the data at low and intermediate p_T, but overshoots them for $p_T > 7$ GeV/c. The D_s^+-meson production tends to be underestimated by the three pQCD calculations in the measured p_T range.

The analysis without decay-vertex reconstruction provides also a direct measurement of the inclusive D^0-meson cross section because no selections are applied on the decay topology, which alter the fraction of prompt and feed-down D mesons. The inclusive D^0-meson cross section is shown in Fig. 12 and compared with results from FONLL calculations [7,8] with the $B \rightarrow D + X$ decay kinematics from the EvtGen package [37]. The contributions of prompt D^0-meson poduction from FONLL and D^0 mesons from B-meson decays from FONLL+EvtGen are also shown separately. The measured cross sections are described by the calculation within the theoretical uncertainties, with the central value of the prediction lying below the data in all the p_T intervals, similarly to what observed for prompt D mesons.

The mean p_T of prompt D^0 mesons, $\langle p_T \rangle$, was evaluated for $p_T > 0$ with a fit of the prompt D^0-meson cross section, that is measured down to $p_T = 0$, using a power-law function, as was done in Ref. [27]. The result is:

$$\langle p_T \rangle_{\text{pp, 5.02 TeV}}^{\text{prompt D}^0} = 2.06 \pm 0.03 \, (\text{stat.}) \pm 0.03 \, (\text{syst.}) \, \text{GeV}/c, \quad (3)$$

which is slightly smaller than the one computed for pp collisions at $\sqrt{s} = 7$ TeV [27]:

$$\langle p_T \rangle_{\text{pp, 7 TeV}}^{\text{prompt D}^0} = 2.19 \pm 0.06 \, (\text{stat.}) \pm 0.04 \, (\text{syst.}) \, \text{GeV}/c. \quad (4)$$
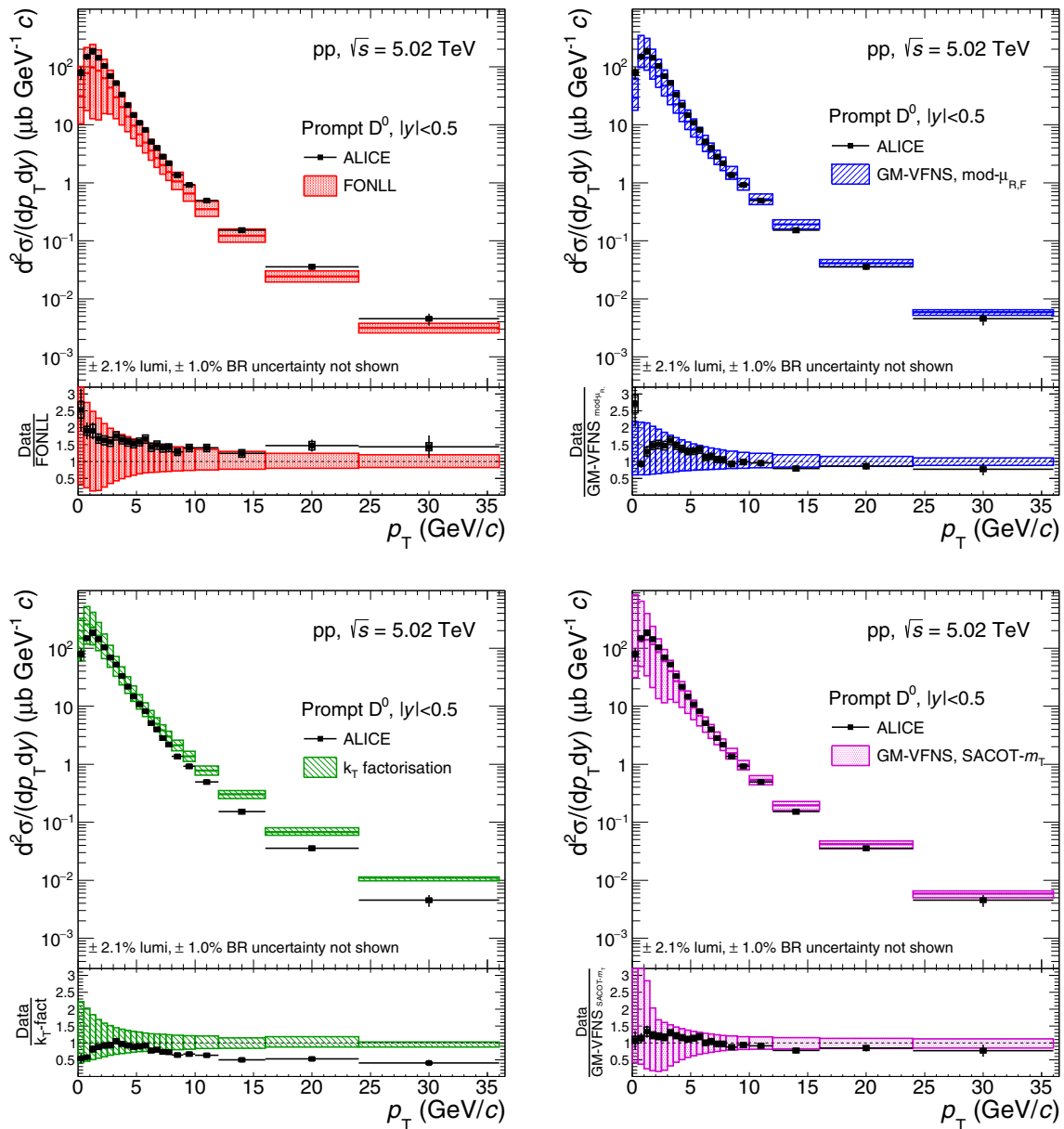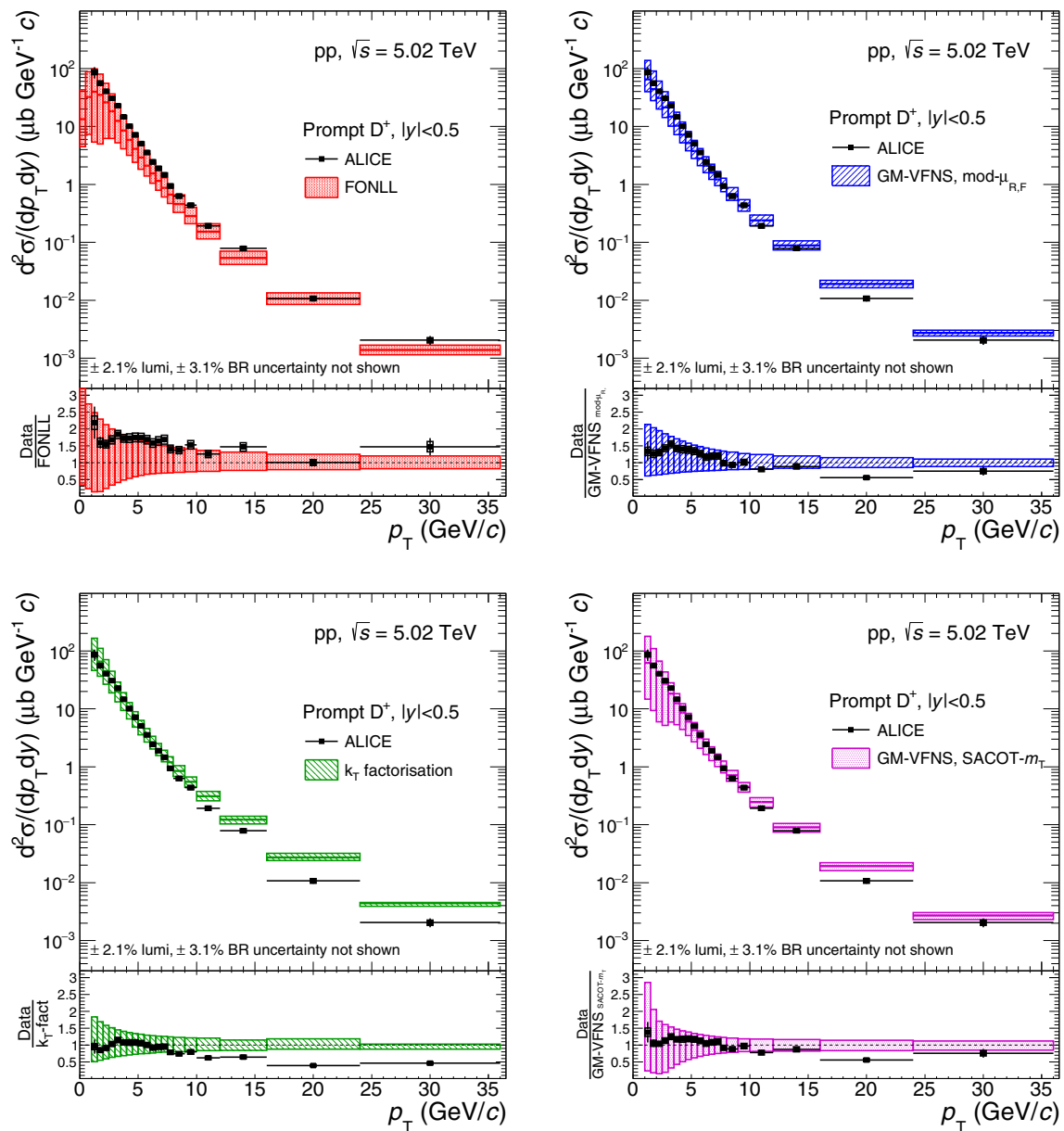
Fig. 8 p_T-differential production cross sections for prompt D^0 meson compared to pQCD calculations: FONLL [7,8], GM-VFNS(mod-$\mu_{R,F}$) [39,40], GM-VFNS(SACOT-m_T) [6], and k_T-factorisation [41]. The ratios of the data to the theoretical predictions are shown in the lower part of each panel

The systematic uncertainty on the $\langle p_T \rangle$ was estimated as described in Refs. [19,27]. The contributions due to the correlated and uncorrelated systematic uncertainties on the measured p_T-differential cross section were taken into account separately and the contribution due to the choice of the fit function has been estimated by comparing results obtained using different functions and using a method based on direct calculations of $\langle p_T \rangle$ from the data points.

5.2 D-meson cross-section ratios

The ratios of the p_T-differential cross sections of prompt D^0, D^+, D^{*+}, and D_s^+ mesons in pp collisions at $\sqrt{s} = 5.02$ TeV are reported in Fig. 13. In the evaluation of the systematic uncertainties on these ratios, the sources of correlated and uncorrelated systematic effects were treated separately. In particular, the contributions of the yield

Fig. 9 p_T-differential production cross sections for prompt D^+ meson compared to pQCD calculations: FONLL [7,8], GM-VFNS(mod-$\mu_{R,F}$) [39,40], GM-VFNS(SACOT-m_T) [6], and k_T-factorisation [41].

The ratios of the data to the theoretical predictions are shown in the lower part of each panel

extraction and cut efficiency were considered as uncorrelated, while those of the feed-down from beauty-hadron decays and the tracking efficiency were treated as fully correlated among the different D-meson species. The measured D-meson cross-section ratios do not show a significant p_T dependence within the experimental uncertainties, thus suggesting no discernible difference between the fragmentation functions of charm quarks to pseudoscalar (D^0, D^+, and D_s^+) and vector (D^{*+}) mesons and to strange and non-strange mesons. The results are compatible within uncer-

tainties with the ratios measured in pp collisions at $\sqrt{s} = 7$ TeV [27].[1]

To study the evolution of prompt D-meson production with the centre-of-mass energy of the collision, the ratios of the production cross sections in pp collisions at $\sqrt{s} = 7$ TeV [27] and $\sqrt{s} = 5.02$ TeV were computed for D^0, D^+,

---

[1] The cross section for D^0 and D^+ mesons in pp collisions at $\sqrt{s} = 7$ TeV were updated with respect to Ref. [27] to account for the change of the world-average BR of $D^0 \rightarrow K^- \pi^+$ and $D^+ \rightarrow K^- \pi^+ \pi^+$ from ($3.93\% \pm 0.04$) to ($3.89\% \pm 0.04$), and from ($9.46\% \pm 0.24$) to ($8.98\% \pm 0.28$), respectively.
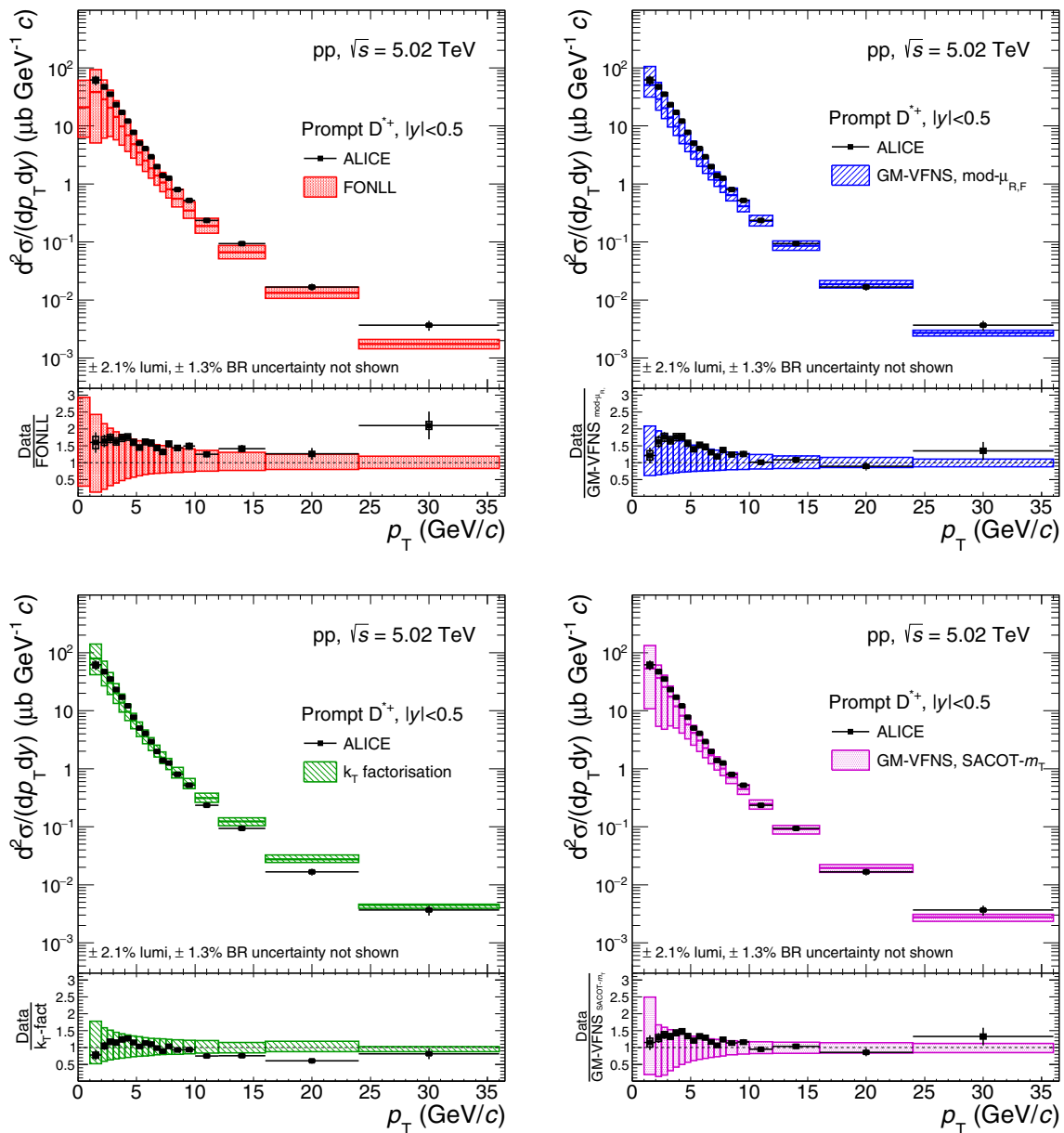
Fig. 10 p_T-differential production cross sections for prompt D^{*+} meson compared to pQCD calculations: FONLL [7,8], GM-VFNS(mod-$\mu_{R,F}$) [39,40], GM-VFNS(SACOT-m_T) [6], and k_T-factorisation [41]. The ratios of the data to the theoretical predictions are shown in the lower part of each panel

D^{*+} and D_s^+ mesons. The systematic uncertainties on the measured ratios were obtained treating the contribution originating from the subtraction of the feed-down from beauty-hadron decays as correlated, while all the other systematic uncertainties on the cross sections were propagated as uncorrelated between the measurements at the two different energies, except for the uncertainty on the BR, which cancels out in the ratio. The results for D^0, D^+, D^{*+} and D_s^+ are compared in Fig. 14, on the left panel. The ratios for the different D-meson species are compatible within uncertainties. In the right panel, the D^0-meson results are compared to FONLL

calculations, which describe consistently the increasing trend as a function of p_T observed in the data. In the FONLL predictions, the uncertainties originating from scale variations and from PDFs cancel out to a large extent in the ratio [24], thus making the magnitude of the theoretical uncertainties comparable with those of the data.

The rapidity dependence of D^0-meson production in pp collisions at $\sqrt{s} = 5.02$ TeV can be studied from the ratios between our measurements at midrapidity and the LHCb results in different y intervals at forward rapidity [22]. The precise measurement of the D^0-meson cross section down
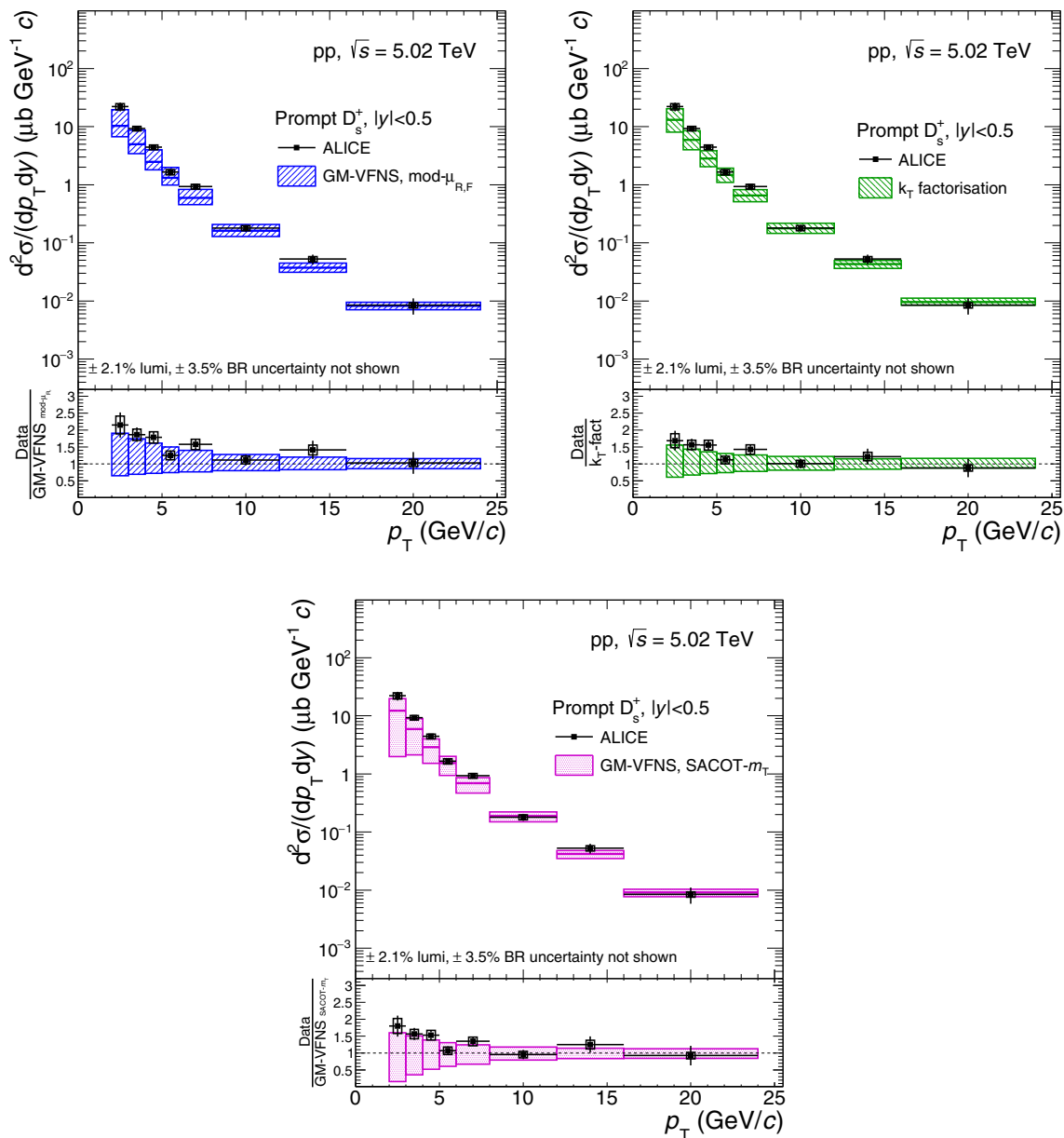
Fig. 11 p_T-differential production cross sections for prompt D_s^+ meson compared to GM-VFNS(mod-$\mu_{R,F}$) [39,40], GM-VFNS(SACOT-m_T) [6], and k_T-factorisation [41] pQCD calculations. The ratios of the data to the theoretical predictions are shown in the lower part of each panel

to $p_T = 0$ presented in this paper, when analysed together with other results at different centre-of-mass energies and rapidities, can provide sensitivity to the gluon PDF at small values of Bjorken-x (10^{-4}–10^{-5}) [24]. In Fig. 15 the ratios of the D^0-meson production cross sections per unit of rapidity measured with ALICE at mid-rapidity ($|y| < 0.5$) and by the LHCb collaboration in three rapidity intervals at forward rapidity $2 < y < 2.5$ (left panel), $3 < y < 3.5$ (middle panel), $4 < y < 4.5$ (right panel) [22] are shown as a function of p_T. The error bars and boxes represent the uncertainty obtained from the propagation of the statistical and systematic uncertainties, respectively, from the p_T-differential cross

sections. The systematic uncertainties, including the one on the luminosity determination, were treated as uncorrelated between the ALICE and LHCb results, except for the uncertainty on the BR, which cancels out in the ratio. The central values and the uncertainties of the FONLL calculations are evaluated as described in Ref. [27]. The measured ratios are described by FONLL calculations, shown as red boxes in Fig. 15. Nevertheless the comparison seems to hint at a different slope in data with respect to FONLL, since at low (high) p_T the data tend to stay above (below) the FONLL central values, in all rapidity intervals.
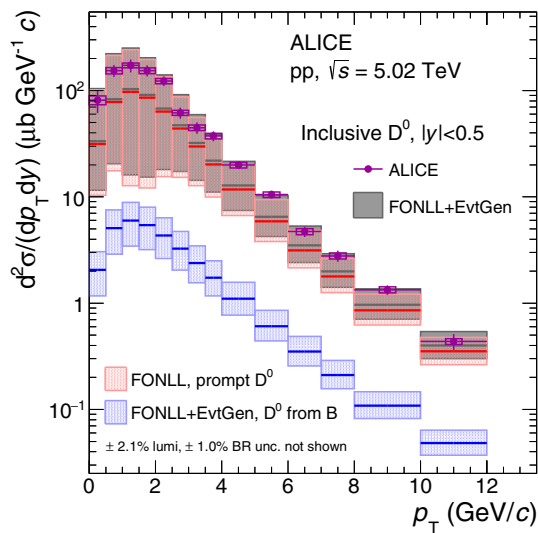
Fig. 12 Inclusive D^0 mesons (including also D^0 mesons from beauty-hadron decays) in $|y| < 0.5$ in pp collisions at $\sqrt{s} = 5.02$ TeV, from the analysis without decay-vertex reconstruction, compared to FONLL pQCD calculations [7,8] with the $B \to D + X$ decay kinematics from the EvtGen package [37] (grey boxes). The contributions of prompt D^0 from FONLL (red) and D^0 from B-meson decays from FONLL+EvtGen (blue) are also shown separately. The vertical error bars and the empty boxes represent the statistical and systematic uncertainties, respectively

5.3 Transverse momentum-integrated cross sections and ratios

The visible production cross sections of prompt D mesons were evaluated by integrating the p_T-differential cross sections over the narrower p_T intervals of the D^+, D^{*+}, and D_s^+-meson measurements, in the measured p_T range. The results are reported in Table 2. The systematic uncertainty was evaluated by propagating all the uncertainties as correlated among p_T intervals, except for the yield extraction uncertainty which is treated as uncorrelated owing to the bin-by-bin variation, significant especially at low p_T, of S/B and background invariant-mass shape.

The ratios of the p_T-integrated yields of the different D-meson species were computed from the cross sections integrated over the common p_T range. The systematic uncertainties on the ratios were computed treating the BR, yield extraction and cut efficiency uncertainties as uncorrelated among the different species and the other sources as correlated. The results are reported in Table 3.

The measured ratios are compatible within uncertainties with the results at $\sqrt{s} = 2.76$ TeV and $\sqrt{s} = 7$ TeV [16,27] and with the measurements of the LHCb collaboration at forward rapidity ($2.0 < y < 4.5$) at three different collision energies $\sqrt{s} = 5.02$, 7, and 13 TeV [21–23].
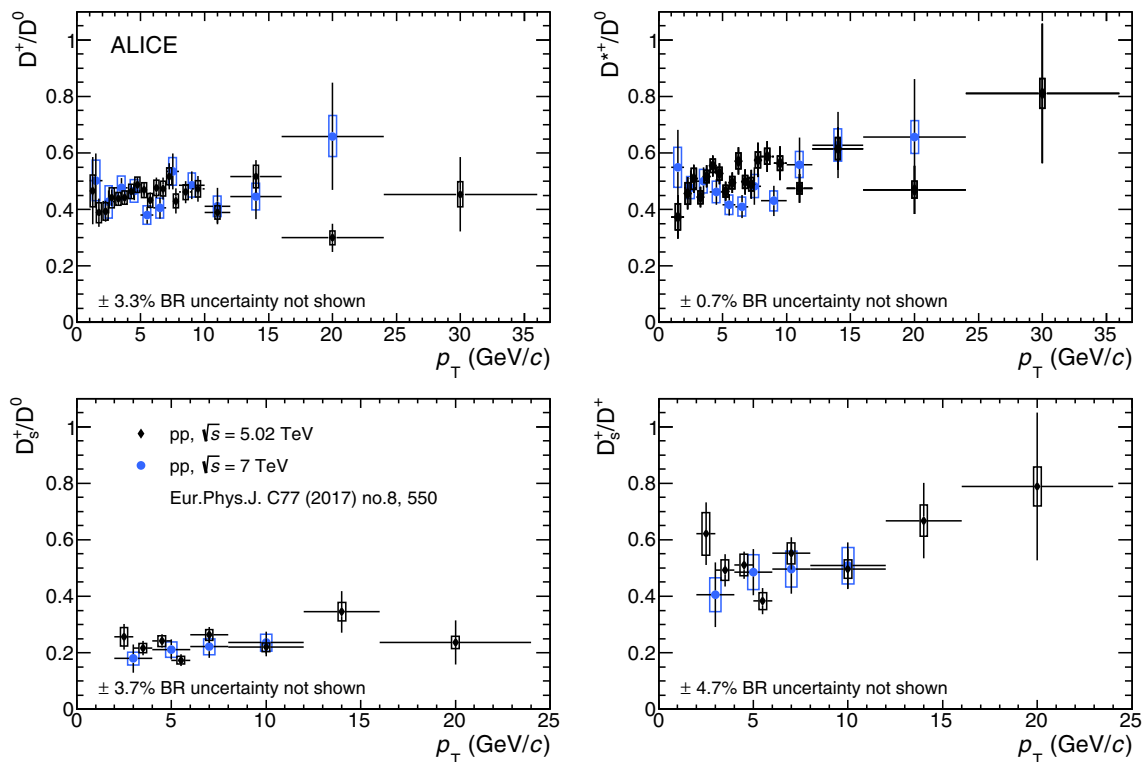
Fig. 13 Ratios of D-meson production cross sections as a function of p_T in pp collisions at $\sqrt{s} = 5.02$ TeV and $\sqrt{s} = 7$ TeV [27]
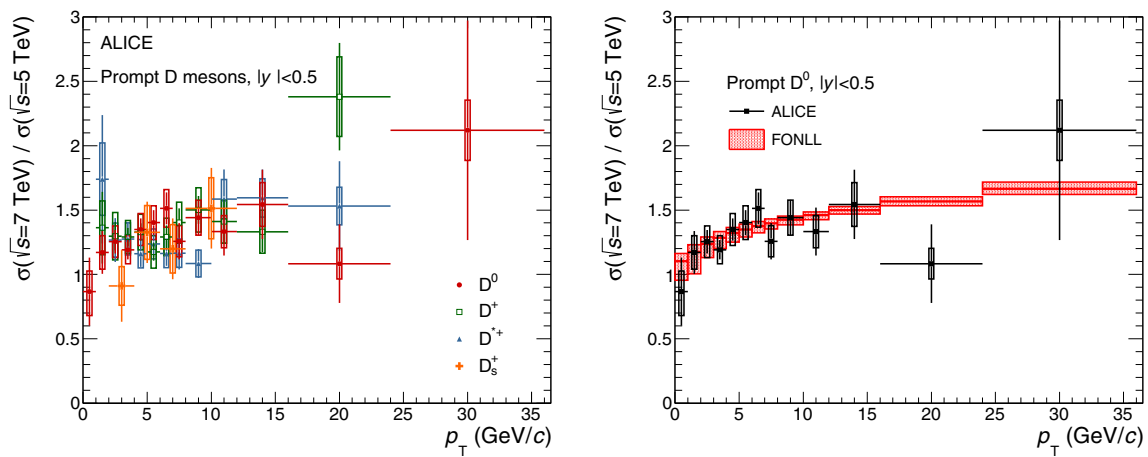
Fig. 14 Ratios of D^0, D^+, D^{*+} and D_s^+-meson production cross sections in pp collisions at $\sqrt{s} = 7$ TeV [27] and $\sqrt{s} = 5.02$ TeV as a function of p_T (left panel). D^0 ratio compared to FONLL pQCD calculations [7,8] (right panel)
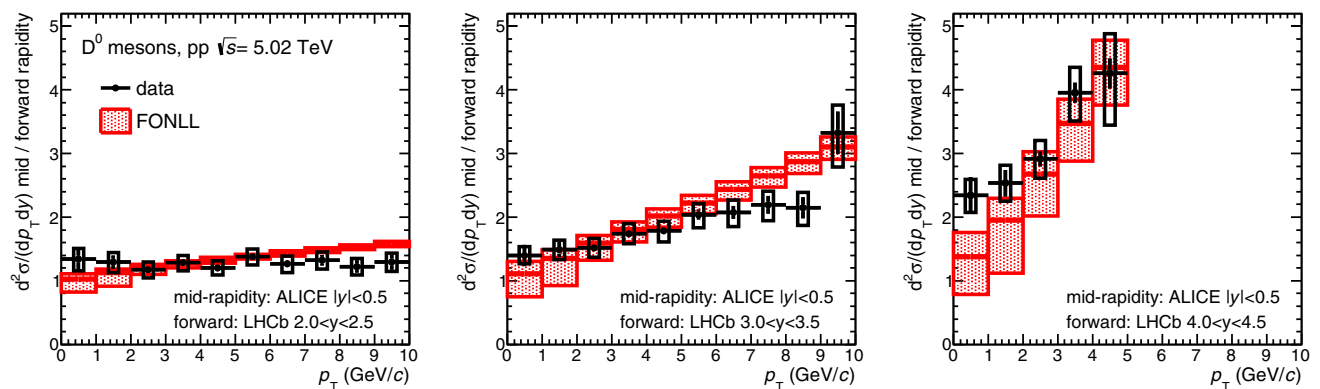
Fig. 15 Ratios of D^0-meson production cross section per unit of rapidity at mid-rapidity ($|y| < 0.5$) to those measured by the LHCb Collaboration [22] in three rapidity ranges, $2 < y < 2.5$ (left panel), $3 < y < 3.5$ (middle panel), and $4 < y < 4.5$ (right panel), as a function of p_T. The error bars and boxes represent the statistical and systematic uncertainty, respectively. Predictions from FONLL calculations are compared to the data points

Table 2 Visible production cross sections of prompt D mesons in $|y| < 0.5$ in pp collisions at $\sqrt{s} = 5.02$ TeV

	Kinematic range	Visible cross section (μb)
D^0	$0 < p_T < 36$ GeV/c	447 ± 20(stat) ± 30(syst) ± 9(lumi) ± 5(BR)
D^+	$1 < p_T < 36$ GeV/c	144 ± 10(stat) ± 10(syst) ± 3(lumi) ± 4(BR)
D^{*+}	$1 < p_T < 36$ GeV/c	143 ± 12(stat) ± 11(syst) ± 3(lumi) ± 2(BR)
D_s^+	$2 < p_T < 24$ GeV/c	40 ± 4(stat) ± 4(syst) ± 1(lumi) ± 1(BR)

Table 3 Ratios of the measured p_T-integrated cross sections of prompt D mesons in $|y| < 0.5$ in pp collisions at $\sqrt{s} = 5.02$ TeV

	Kinematic range	Production cross section ratio
$\sigma(D^+)/\sigma(D^0)$	$1 < p_T < 36$ GeV/c	0.43 ± 0.04(stat) ± 0.03(syst) ± 0.01(BR)
$\sigma(D^{*+})/\sigma(D^0)$	$1 < p_T < 36$ GeV/c	0.43 ± 0.04(stat) ± 0.03(syst) ± 0.003(BR)
$\sigma(D_s^+)/\sigma(D^0)$	$2 < p_T < 24$ GeV/c	0.24 ± 0.02(stat) ± 0.02(syst) ± 0.01(BR)
$\sigma(D_s^+)/\sigma(D^+)$	$2 < p_T < 24$ GeV/c	0.56 ± 0.06(stat) ± 0.05(syst) ± 0.03(BR)

Table 4 Production cross sections of prompt D mesons in $|y| < 0.5$ and full p_T range in pp collisions at $\sqrt{s} = 5.02$ TeV

	Extr. factor to $p_T > 0$	$d\sigma/dy \,|_{|y|<0.5}$ (μb)
D^0	$1.0000^{+0.0003}_{-0.0000}$	$447 \pm 20(\text{stat}) \pm 30(\text{syst}) \pm 9(\text{lumi}) \pm 5(\text{BR})$
D^+	$1.28^{+0.35}_{-0.09}$	$184 \pm 13(\text{stat}) \pm 13(\text{syst}) \pm 4(\text{lumi}) \pm 6(\text{BR})^{+50}_{-13}(\text{extrap})$
D^{*+}	$1.24^{+0.34}_{-0.08}$	$178 \pm 15(\text{stat}) \pm 14(\text{syst}) \pm 4(\text{lumi}) \pm 2(\text{BR})^{+48}_{-12}(\text{extrap})$
D_s^+	$2.35^{+0.78}_{-0.66}$	$95 \pm 9(\text{stat}) \pm 10(\text{syst}) \pm 2(\text{lumi}) \pm 3(\text{BR})^{+31}_{-26}(\text{extrap})$

The production cross sections per unit of rapidity, $d\sigma/dy$, at mid-rapidity were computed for each D-meson species by extrapolating the visible cross section to the full p_T range. The extrapolation factor for a given D-meson species was computed using the FONLL central parameters to evaluate the ratio between the total production cross section in $|y| < 0.5$ and that in the experimentally covered phase space. It was verified that the extrapolation factors computed with FONLL were compatible with those resulting from GM-VFNS calculations. The systematic uncertainty on the extrapolation factor was estimated as proposed in Ref. [8], considering sources due to (i) the CTEQ6.6 PDFs uncertainties [42], (ii) the variation of the charm-quark mass and (iii) the renormalisation and factorisation scales in the FONLL calculation. For D^0 mesons, for which the measurement extends down to $p_T = 0$, the extrapolation factor accounts only for the very small contribution of D mesons with $p_T > 36$ GeV/c and therefore its value is very close to unity with negligible uncertainty. The FONLL predictions are not available for D_s^+ mesons, hence in this case the central value of the extrapolation factor was computed as described in Ref. [27], combining the prediction based on the p_T-differential cross section of charm quarks from FONLL, the fractions $f(c \to D_s^+)$ and $f(c \to D_s^{*+})$ from ALEPH [46], and the fragmentation functions from Ref. [47], which have one parameter, r, that was set to 0.1 as done in FONLL [48]. An additional contribution to the systematic uncertainty was assigned based on the envelope of the results obtained using the FONLL p_T-differential cross sections of non-strange D mesons to compute the D_s^+-meson extrapolation factor. The computed extrapolation factors and the prompt D-meson production cross sections per unit of rapidity $d\sigma/dy$ in $|y| < 0.5$, are presented in Table 4.

In Ref. [27], the $c\bar{c}$ production cross section per unit of rapidity at mid-rapidity ($|y| < 0.5$) and the total charm production cross sections in pp collisions at $\sqrt{s} = 7$ TeV were reported. They were computed from the prompt D^0-meson production cross section, which was divided by the fraction of charm quarks hadronising into D^0 mesons, $f(c \to D^0) = 0.542 \pm 0.024$, derived in Ref. [49] by averaging the measurements in e^+e^- collisions at LEP. However, recent measurements of the Λ_c^+ baryon production cross section in pp collisions at $\sqrt{s} = 7$ TeV and in p–Pb collisions at $\sqrt{s} = 5.02$ TeV [50] show a significant enhancement of

the Λ_c^+/D^0 ratio for $p_T > 1$ GeV/c as compared to the values measured in e^+e^- and ep collisions at lower centre-of-mass energies. This suggests that the fragmentation fractions of charm quarks into charmed baryons in pp collisions at LHC energies might differ significantly from the LEP results reported in Ref. [49] and that measurements of charmed-baryon production cross sections in pp collisions at $\sqrt{s} = 5.02$ TeV are needed for an accurate calculation of the charm production cross section.

6 Summary

We have reported the measurement of the inclusive p_T-differential production cross sections of prompt D^0, D^+, D^{*+}, and D_s^+ mesons at mid-rapidity ($|y| < 0.5$) in pp collisions at a centre-of-mass energy of $\sqrt{s} = 5.02$ TeV, obtained with the data collected at the end of 2017 with the ALICE detector. The measurement was performed in the transverse-momentum range $0 < p_T < 36$ GeV/c for D^0, $1 < p_T < 36$ GeV/c for D^+ and D^{*+}, and $2 < p_T < 24$ GeV/c for D_s^+ mesons. It is measured in finer p_T bins with respect to the previous measurements at $\sqrt{s} = 7$ TeV [27], providing a more detailed description of the cross-section p_T shape. The results were compared and found compatible with different pQCD calculations performed with different schemes: FONLL [7,8], two calculations using the GM-VNFS framework with different prescriptions [6,39,40], and a calculation based on k_T-factorisation [41]. The ratios of D^0-meson production cross sections measured with ALICE and LHCb in different rapidity intervals were compatible with FONLL calculations, indicating a slightly smaller slope in data with respect to theoretical predictions. The ratios of the cross sections of D^0, D^+, and D^{*+} mesons at $\sqrt{s} = 7$ TeV [27] and $\sqrt{s} = 5.02$ TeV are consistent with FONLL pQCD calculations. The ratios of the p_T-differential cross sections of D^0, D^+, D^{*+}, and D_s^+ mesons were found to be compatible within uncertainties with the D-meson cross-section ratios measured in pp collisions at $\sqrt{s} = 7$ TeV [27]. The new measurement will allow for a more accurate determination of the nuclear modification factor R_{pA} in p–Pb collisions and R_{AA} in Pb–Pb collisions at $\sqrt{s_{NN}} = 5.02$ TeV, due to

the larger statistics available and since it is performed at the same centre-of-mass energy of the other collision systems.

Data Availability Statement This manuscript has associated data in a data repository. [Authors' comment: The numerical values of the data points will be uploaded to HEPData.]

References

1. J.C. Collins, D.E. Soper, G.F. Sterman, Factorization of hard processes in QCD. Adv. Ser. Direct. High Energy Phys. **5**, 1–91 (1989). arXiv:hep-ph/0409313 [hep-ph]
2. S. Catani, M. Ciafaloni, F. Hautmann, High-energy factorization and small x heavy flavor production. Nucl. Phys. B **366**, 135–188 (1991)
3. B.A. Kniehl, G. Kramer, I. Schienbein, H. Spiesberger, Inclusive D*+- production in p anti-p collisions with massive charm quarks. Phys. Rev. D **71**, 014018 (2005). arXiv:hep-ph/0410289 [hep-ph]
4. B.A. Kniehl, G. Kramer, I. Schienbein, H. Spiesberger, Collinear subtractions in hadroproduction of heavy quarks. Eur. Phys. J. C **41**, 199–212 (2005). arXiv:hep-ph/0502194 [hep-ph]
5. B.A. Kniehl, G. Kramer, I. Schienbein, H. Spiesberger, Inclusive Charmed–Meson production at the CERN LHC. Eur. Phys. J. C **72**, 2082 (2012). arXiv:1202.0439 [hep-ph]
6. I. Helenius, H. Paukkunen, Revisiting the D-meson hadroproduction in general-mass variable flavour number scheme. JHEP **05**, 196 (2018). arXiv:1804.03557 [hep-ph]
7. M. Cacciari, M. Greco, P. Nason, The p_T spectrum in heavy flavor hadroproduction. JHEP **05**, 007 (1998). arXiv:hep-ph/9803400 [hep-ph]
8. M. Cacciari, S. Frixione, N. Houdeau, M.L. Mangano, P. Nason, G. Ridolfi, Theoretical predictions for charm and bottom production at the LHC. JHEP **10**, 137 (2012). arXiv:1205.6344 [hep-ph]
9. M. Luszczak, R. Maciula, A. Szczurek, Nonphotonic electrons at RHIC within k(t)-factorization approach and with experimental semileptonic decay functions. Phys. Rev. D **79**, 034009 (2009). arXiv:0807.5044 [hep-ph]
10. R. Maciula, A. Szczurek, Open charm production at the LHC - k_t-factorization approach. Phys. Rev. D **87**(9), 094022 (2013). arXiv:1301.3033 [hep-ph]
11. A. Andronic et al., Heavy-flavour and quarkonium production in the LHC era: from proton–proton to heavy-ion collisions. Eur. Phys. J. C **76**(3), 107 (2016). arXiv:1506.03981 [nucl-ex]
12. STAR Collaboration, L. Adamczyk et al., Measurements of D^0 and D^{*+} production in pp collisions at $\sqrt{s}$ = 200 GeV. Phys. Rev. D **86**, 072013 (2012). arXiv:1204.4244 [nucl-ex]
13. CDF Collaboration, D. Acosta et al., Measurement of prompt charm meson production cross sections in $p\bar{p}$ collisions at

$\sqrt{s}$ = 1.96 TeV. Phys. Rev. Lett. **91**, 241804 (2003). arXiv:hep-ex/0307080 [hep-ex]

14. ATLAS Collaboration, G. Aad et al., Measurement of $D^{*\pm}$, $D^{\pm}$ and $D_s^{\pm}$ meson production cross sections in pp collisions at $\sqrt{s} = 7$ TeV with the ATLAS detector. Nucl. Phys. B **907**, 717-763 (2016). arXiv:1512.02913 [hep-ex]

15. ALICE Collaboration, B. Abelev et al., Measurement of charm production at central rapidity in proton–proton collisions at $\sqrt{s} = 7$ TeV. JHEP **01**, 128 (2012). arXiv:1111.1553 [hep-ex]

16. ALICE Collaboration, B. Abelev et al., Measurement of charm production at central rapidity in proton–proton collisions at $\sqrt{s} = 2.76$ TeV. JHEP **07**, 191 (2012). arXiv:1205.4007 [hep-ex]

17. ALICE Collaboration, B. Abelev et al., Measurement of electrons from semileptonic heavy-flavour hadron decays in pp collisions at $\sqrt{s} = 7\,TeV$. Phys. Rev. D **86**, 112007 (2012). arXiv:1205.5423 [hep-ex]

18. ALICE Collaboration, B. Abelev et al., D_s^+ meson production at central rapidity in proton–proton collisions at $\sqrt{s} = 7$ TeV. Phys. Lett. B **718**, 279-294 (2012). arXiv:1208.1948 [hep-ex]

19. ALICE Collaboration, J. Adam et al., D-meson production in p-Pb collisions at $\sqrt{s_{NN}} = 5.02$ TeV and in pp collisions at $\sqrt{s} = 7$ TeV. Phys. Rev. C **94**(5), 054908 (2016). arXiv:1605.07569 [nucl-ex]

20. CMS Collaboration, A.M. Sirunyan et al., Nuclear modification factor of D^0 mesons in PbPb collisions at $\sqrt{s_{NN}} = 5.02$ TeV. Phys. Lett. B **782**, 474–496 (2018). arXiv:1708.04962 [nucl-ex]

21. LHCb Collaboration, R. Aaij et al., Prompt charm production in pp collisions at $\sqrt{s} = 7$ TeV. Nucl. Phys. B **871**, 1–20 (2013). arXiv:1302.2864 [hep-ex]

22. LHCb Collaboration, R. Aaij et al., Measurements of prompt charm production cross-sections in pp collisions at $\sqrt{s} = 5$ TeV. JHEP **06**, 147 (2017). arXiv:1610.02230 [hep-ex]

23. LHCb Collaboration, R. Aaij et al., Measurements of prompt charm production cross-sections in pp collisions at $\sqrt{s} = 13$ TeV. JHEP **03**, 159 (2016). arXiv:1510.01707 [hep-ex]. [Erratum: *JHEP***09** (2016) 013]

24. M. Cacciari, M.L. Mangano, P. Nason, Gluon PDF constraints from the ratio of forward heavy-quark production at the LHC at $\sqrt{s} = 7$ and 13 TeV. Eur. Phys. J. C **75**(12), 610 (2015). arXiv:1507.06197 [hep-ph]

25. F. Prino, R. Rapp, Open heavy flavor in QCD matter and in nuclear collisions. J. Phys. **G43**(9), 093002 (2016). arXiv:1603.00529 [nucl-ex]

26. G. Aarts et al., Heavy-flavor production and medium properties in high-energy nuclear collisions—what next? Eur. Phys. J. A **53**(5), 93 (2017). arXiv:1612.08032 [nucl-th]

27. ALICE Collaboration, S. Acharya et al., Measurement of D-meson production at mid-rapidity in pp collisions at $\sqrt{s} = 7$ TeV. Eur. Phys. J. C **77**(8), 550 (2017). arXiv:1702.00766 [hep-ex]

28. ALICE Collaboration, K. Aamodt et al., The ALICE experiment at the CERN LHC. JINST **3**, S08002 (2008)

29. ALICE Collaboration, B.B. Abelev et al., Performance of the ALICE Experiment at the CERN LHC. Int. J. Mod. Phys. A **29**, 1430044 (2014). arXiv:1402.4476 [nucl-ex]

30. Particle Data Group Collaboration, M. Tanabashi et al., Review of particle physics. Phys. Rev. D **98**(3), 030001 (2018)

31. ALICE Collaboration, S. Acharya et al., Measurement of D^0, D^+, D^{*+} and D_s^+ production in Pb-Pb collisions at $\sqrt{s_{NN}} = 5.02$ TeV. Submitted to: JHEP (2018). arXiv:1804.09083 [nucl-ex]

32. ALICE Collaboration Collaboration, ALICE 2017 luminosity determination for pp collisions at $\sqrt{s} = 5$ TeV. http://cds.cern.ch/record/2648933

33. T. Sjostrand, S. Mrenna, P.Z. Skands, PYTHIA 6.4 physics and manual. JHEP **05**, 026 (2006). arXiv:hep-ph/0603175 [hep-ph]

34. P.Z. Skands, Tuning Monte Carlo Generators: the Perugia Tunes. Phys. Rev. D **82**, 074018 (2010). arXiv:1005.3457 [hep-ph]

35. R. Brun, F. Carminati, S. Giani, CERN Program Library Long Write-up, W5013 GEANT Detector Description and Simulation Tool. Tech. Rep. CERN-W-5013 (1994)

36. M. Cacciari, S. Frixione, P. Nason, The p(T) spectrum in heavy flavor photoproduction. JHEP **03**, 006 (2001). arXiv:hep-ph/0102134 [hep-ph]

37. D.J. Lange, The EvtGen particle decay simulation package. Nucl. Instrum. Meth. **A462**, 152–155 (2001)

38. ALICE Collaboration, The ALICE definition of primary particles (2017). https://cds.cern.ch/record/2270008. ALICE-PUBLIC-2017-005

39. M. Benzke, M.V. Garzelli, B. Kniehl, G. Kramer, S. Moch, G. Sigl, Prompt neutrinos from atmospheric charm in the general-mass variable-flavor-number scheme. JHEP **12**, 021 (2017). arXiv:1705.10386 [hep-ph]

40. G. Kramer, H. Spiesberger, Study of heavy meson production in pPb collisions at $\sqrt{s}= 5.02$ TeV in the general-mass variable-flavour-number scheme. Nucl. Phys. B **925**, 415–430 (2017). arXiv:1703.04754 [hep-ph]

41. R. Maciula, A. Szczurek, Production of Λ_c baryons at the LHC within the k_T-factorization approach and independent parton fragmentation picture. Phys. Rev. D **98**(1), 014016 (2018). arXiv:1803.05807 [hep-ph]

42. J. Pumplin, D.R. Stump, J. Huston, H.L. Lai, P.M. Nadolsky, W.K. Tung, New generation of parton distributions with uncertainties from global QCD analysis. JHEP **07**, 012 (2002). arXiv:hep-ph/0201195 [hep-ph]

43. S. Dulat, T.-J. Hou, J. Gao, M. Guzzi, J. Huston, P. Nadolsky, J. Pumplin, C. Schmidt, D. Stump, C.P. Yuan, New parton distribution functions from a global analysis of quantum chromodynamics. Phys. Rev. D **93**(3), 033006 (2016). arXiv:1506.07443 [hep-ph]

44. NNPDF Collaboration, R.D. Ball et al., Parton distributions from high-precision collider data. Eur. Phys. J. C **77**(10), 663 (2017). arXiv:1706.00428 [hep-ph]

45. L.A. Harland-Lang, A.D. Martin, P. Motylinski, R.S. Thorne, Parton distributions in the LHC era: MMHT 2014 PDFs. Eur. Phys. J. C **75**(5), 204 (2015). arXiv:1412.3989 [hep-ph]

46. ALEPH Collaboration, R. Barate et al., Study of charm production in Z decays. Eur. Phys. J. C **16**, 597–611 (2000). arXiv:hep-ex/9909032 [hep-ex]

47. E. Braaten, K.-M. Cheung, S. Fleming, T.C. Yuan, Perturbative QCD fragmentation functions as a model for heavy quark fragmentation. Phys. Rev. D **51**, 4819–4829 (1995). arXiv:hep-ph/9409316 [hep-ph]

48. M. Cacciari, P. Nason, Charm cross-sections for the Tevatron Run II. JHEP **09**, 006 (2003). arXiv:hep-ph/0306212 [hep-ph]

49. L. Gladilin, Fragmentation fractions of c and b quarks into charmed hadrons at LEP. Eur. Phys. J. C **75**(1), 19 (2015). arXiv:1404.3888 [hep-ex]

50. ALICE Collaboration, S. Acharya et al., Λ_c^+ production in pp collisions at $\sqrt{s} = 7$ TeV and in p-Pb collisions at $\sqrt{s_{NN}} = 5.02$ TeV. JHEP **04**, 108 (2018). arXiv:1712.09581 [nucl-ex]

ALICE Collaboration

S. Acharya[140], D. Adamová[93], S. P. Adhya[140], A. Adler[74], J. Adolfsson[80], M. M. Aggarwal[98], G. Aglieri Rinella[34], M. Agnello[31], Z. Ahammed[140], S. Ahmad[17], S. U. Ahn[76], S. Aiola[145], A. Akindinov[64], M. Al-Turany[104], S. N. Alam[140], D. S. D. Albuquerque[121], D. Aleksandrov[87], B. Alessandro[58], H. M. Alfanda[6], R. Alfaro Molina[72], B. Ali[17], Y. Ali[15], A. Alici[10,27,53], A. Alkin[2], J. Alme[22], T. Alt[69], L. Altenkamper[22], I. Altsybeev[111], M. N. Anaam[6], C. Andrei[47], D. Andreou[34], H. A. Andrews[108], A. Andronic[104,143], M. Angeletti[34], V. Anguelov[102], C. Anson[16], T. Antičić[105], F. Antinori[56], P. Antonioli[53], R. Anwar[125], N. Apadula[79], L. Aphecetche[113], H. Appelshäuser[69], S. Arcelli[27], R. Arnaldi[58], M. Arratia[79], I. C. Arsene[21], M. Arslandok[102], A. Augustinus[34], R. Averbeck[104], M. D. Azmi[17], A. Badalà[55], Y. W. Baek[40,60], S. Bagnasco[58], R. Bailhache[69], R. Bala[99], A. Baldisseri[136], M. Ball[42], R. C. Baral[85], R. Barbera[28], L. Barioglio[26], G. G. Barnaföldi[144], L. S. Barnby[92], V. Barret[133], P. Bartalini[6], K. Barth[34], E. Bartsch[69], N. Bastid[133], S. Basu[142], G. Batigne[113], B. Batyunya[75], P. C. Batzing[21], D. Bauri[48], J. L. Bazo Alba[109], I. G. Bearden[88], C. Bedda[63], N. K. Behera[60], I. Belikov[135], F. Bellini[34], H. Bello Martinez[44], R. Bellwied[125], L. G. E. Beltran[119], V. Belyaev[91], G. Bencedi[144], S. Beole[26], A. Bercuci[47], Y. Berdnikov[96], D. Berenyi[144], R. A. Bertens[129], D. Berzano[58], L. Betev[34], A. Bhasin[99], I. R. Bhat[99], H. Bhatt[48], B. Bhattacharjee[41], A. Bianchi[26], L. Bianchi[26,125], N. Bianchi[51], J. Bielčík[37], J. Bielčíková[93], A. Bilandzic[103,116], G. Biro[144], R. Biswas[3], S. Biswas[3], J. T. Blair[118], D. Blau[87], C. Blume[69], G. Boca[138], F. Bock[34], A. Bogdanov[91], L. Boldizsár[144], A. Bolozdynya[91], M. Bombara[38], G. Bonomi[139], M. Bonora[34], H. Borel[136], A. Borissov[102,143], M. Borri[127], E. Botta[26], C. Bourjau[88], L. Bratrud[69], P. Braun-Munzinger[104], M. Bregant[120], T. A. Broker[69], M. Broz[37], E. J. Brucken[43], E. Bruna[58], G. E. Bruno[33], M. D. Buckland[127], D. Budnikov[106], H. Buesching[69], S. Bufalino[31], P. Buhler[112], P. Buncic[34], O. Busch[132,a], Z. Buthelezi[73], J. B. Butt[15], J. T. Buxton[95], D. Caffarri[89], H. Caines[145], A. Caliva[104], E. Calvo Villar[109], R. S. Camacho[44], P. Camerini[25], A. A. Capon[112], F. Carnesecchi[10,27], J. Castillo Castellanos[136], A. J. Castro[129], E. A. R. Casula[54], C. Ceballos Sanchez[52], P. Chakraborty[48], S. Chandra[140], B. Chang[126], W. Chang[6], S. Chapeland[34], M. Chartier[127], S. Chattopadhyay[140], S. Chattopadhyay[107], A. Chauvin[24], C. Cheshkov[134], B. Cheynis[134], V. Chibante Barroso[34], D. D. Chinellato[121], S. Cho[60], P. Chochula[34], T. Chowdhury[133], P. Christakoglou[89], C. H. Christensen[88], P. Christiansen[80], T. Chujo[132], C. Cicalo[54], L. Cifarelli[10,27], F. Cindolo[53], J. Cleymans[124], F. Colamaria[52], D. Colella[52], A. Collu[79], M. Colocci[27], M. Concas[58,b], G. Conesa Balbastre[78], Z. Conesa del Valle[61], G. Contin[127], J. G. Contreras[37], T. M. Cormier[94], Y. Corrales Morales[26,58], P. Cortese[32], M. R. Cosentino[122], F. Costa[34], S. Costanza[138], J. Crkovská[61], P. Crochet[133], E. Cuautle[70], L. Cunqueiro[94], D. Dabrowski[141], T. Dahms[103,116], A. Dainese[56], F. P. A. Damas[113,136], S. Dani[66], M. C. Danisch[102], A. Danu[68], D. Das[107], I. Das[107], S. Das[3], A. Dash[85], S. Dash[48], A. Dashi[103], S. De[49,85], A. De Caro[30], G. de Cataldo[52], C. de Conti[120], J. de Cuveland[39], A. De Falco[24], D. De Gruttola[10,30], N. De Marco[58], S. De Pasquale[30], R. D. De Souza[121], H. F. Degenhardt[120], A. Deisting[102,104], K. R. Deja[141], A. Deloff[84], S. Delsanto[26], P. Dhankher[48], D. Di Bari[33], A. Di Mauro[34], R. A. Diaz[8], T. Dietel[124], P. Dillenseger[69], Y. Ding[6], R. Divià[34], Ø. Djuvsland[22], A. Dobrin[34], D. Domenicis Gimenez[120], B. Dönigus[69], O. Dordic[21], A. K. Dubey[140], A. Dubla[104], S. Dudi[98], A. K. Duggal[98], M. Dukhishyam[85], P. Dupieux[133], R. J. Ehlers[145], D. Elia[52], H. Engel[74], E. Epple[145], B. Erazmus[113], F. Erhardt[97], A. Erokhin[111], M. R. Ersdal[22], B. Espagnon[61], G. Eulisse[34], J. Eum[18], D. Evans[108], S. Evdokimov[90], L. Fabbietti[103,116], M. Faggin[29], J. Faivre[78], A. Fantoni[51], M. Fasel[94], L. Feldkamp[143], A. Feliciello[58], G. Feofilov[111], A. Fernández Téllez[44], A. Ferrero[136], A. Ferretti[26], A. Festanti[34], V. J. G. Feuillard[102], J. Figiel[117], S. Filchagin[106], D. Finogeev[62], F. M. Fionda[22], G. Fiorenza[52], F. Flor[125], S. Foertsch[73], P. Foka[104], S. Fokin[87], E. Fragiacomo[59], A. Francisco[113], U. Frankenfeld[104], G. G. Fronze[26], U. Fuchs[34], C. Furget[78], A. Furs[62], M. Fusco Girard[30], J. J. Gaardhøje[88], M. Gagliardi[26], A. M. Gago[109], K. Gajdosova[37,88], A. Gal[135], C. D. Galvan[119], P. Ganoti[83], C. Garabatos[104], E. Garcia-Solis[11], K. Garg[28], C. Gargiulo[34], K. Garner[143], P. Gasik[103,116], E. F. Gauger[118], M. B. Gay Ducati[71], M. Germain[113], J. Ghosh[107], P. Ghosh[140], S. K. Ghosh[3], P. Gianotti[51], P. Giubellino[58,104], P. Giubilato[29], P. Glässel[102], D. M. Goméz Coral[72], A. Gomez Ramirez[74], V. Gonzalez[104], P. González-Zamora[44], S. Gorbunov[39], L. Görlich[117], S. Gotovac[35], V. Grabski[72], L. K. Graczykowski[141], K. L. Graham[108], L. Greiner[79], A. Grelli[63], C. Grigoras[34], V. Grigoriev[91], A. Grigoryan[1], S. Grigoryan[75], J. M. Gronefeld[104], F. Grosa[31], J. F. Grosse-Oetringhaus[34], R. Grosso[104], R. Guernane[78], B. Guerzoni[27], M. Guittiere[113], K. Gulbrandsen[88], T. Gunji[131], A. Gupta[99], R. Gupta[99], I. B. Guzman[44], R. Haake[34,145], M. K. Habib[104], C. Hadjidakis[61], H. Hamagaki[81], G. Hamar[144], M. Hamid[6], J. C. Hamon[135], R. Hannigan[118], M. R. Haque[63], A. Harlenderova[104], J. W. Harris[145], A. Harton[11], H. Hassan[78], D. Hatzifotiadou[10,53], P. Hauer[42], S. Hayashi[131], S. T. Heckel[69], E. Hellbär[69], H. Helstrup[36], A. Herghelegiu[47], E. G. Hernandez[44], G. Herrera Corral[9], F. Herrmann[143], K. F. Hetland[36], T. E. Hilden[43], H. Hillemanns[34], C. Hills[127], B. Hippolyte[135], B. Hohlweger[103], D. Horak[37], S. Hornung[104], R. Hosokawa[132], J. Hota[66], P. Hristov[34], C. Huang[61], C. Hughes[129], P. Huhn[69], T. J. Humanic[95], H. Hushnud[107], L. A. Husova[143], N. Hussain[41], S. A. Hussain[15], T. Hussain[17], D. Hutter[39], D. S. Hwang[19], J. P. Iddon[127], R. Ilkaev[106], M. Inaba[132], M. Ippolitov[87], M. S. Islam[107], M. Ivanov[104],

V. Ivanov[96], V. Izucheev[90], B. Jacak[79], N. Jacazio[27], P. M. Jacobs[79], M. B. Jadhav[48], S. Jadlovska[115], J. Jadlovsky[115], S. Jaelani[63], C. Jahnke[120], M. J. Jakubowska[141], M. A. Janik[141], M. Jercic[97], O. Jevons[108], R. T. Jimenez Bustamante[104], M. Jin[125], P. G. Jones[108], A. Jusko[108], P. Kalinak[65], A. Kalweit[34], J. H. Kang[146], V. Kaplin[91], S. Kar[6], A. Karasu Uysal[77], O. Karavichev[62], T. Karavicheva[62], P. Karczmarczyk[34], E. Karpechev[62], U. Kebschull[74], R. Keidel[46], M. Keil[34], B. Ketzer[42], Z. Khabanova[89], A. M. Khan[6], S. Khan[17], S. A. Khan[140], A. Khanzadeev[96], Y. Kharlov[90], A. Khatun[17], A. Khuntia[49], B. Kileng[36], B. Kim[60], B. Kim[132], D. Kim[146], D. J. Kim[126], E. J. Kim[13], H. Kim[146], J. S. Kim[40], J. Kim[102], J. Kim[146], J. Kim[13], M. Kim[60,102], S. Kim[19], T. Kim[146], T. Kim[146], K. Kindra[98], S. Kirsch[39], I. Kisel[39], S. Kiselev[64], A. Kisiel[141], J. L. Klay[5], C. Klein[69], J. Klein[58], S. Klein[79], C. Klein-Bösing[143], S. Klewin[102], A. Kluge[34], M. L. Knichel[34], A. G. Knospe[125], C. Kobdaj[114], M. Kofarago[144], M. K. Köhler[102], T. Kollegger[104], A. Kondratyev[75], N. Kondratyeva[91], E. Kondratyuk[90], P. J. Konopka[34], M. Konyushikhin[142], L. Koska[115], O. Kovalenko[84], V. Kovalenko[111], M. Kowalski[117], I. Králik[65], A. Kravčáková[38], L. Kreis[104], M. Krivda[65,108], F. Krizek[93], M. Krüger[69], E. Kryshen[96], M. Krzewicki[39], A. M. Kubera[95], V. Kučera[60,93], C. Kuhn[135], P. G. Kuijer[89], L. Kumar[98], S. Kumar[48], S. Kundu[85], P. Kurashvili[84], A. Kurepin[62], A. B. Kurepin[62], S. Kushpil[93], J. Kvapil[108], M. J. Kweon[60], Y. Kwon[146], S. L. La Pointe[39], P. La Rocca[28], Y. S. Lai[79], R. Langoy[123], K. Lapidus[34,145], A. Lardeux[21], P. Larionov[51], E. Laudi[34], R. Lavicka[37], T. Lazareva[111], R. Lea[25], L. Leardini[102], S. Lee[146], F. Lehas[89], S. Lehner[112], J. Lehrbach[39], R. C. Lemmon[92], I. León Monzón[119], P. Lévai[144], X. Li[12], X. L. Li[6], J. Lien[123], R. Lietava[108], B. Lim[18], S. Lindal[21], V. Lindenstruth[39], S. W. Lindsay[127], C. Lippmann[104], M. A. Lisa[95], V. Litichevskyi[43], A. Liu[79], H. M. Ljunggren[80], W. J. Llope[142], D. F. Lodato[63], V. Loginov[91], C. Loizides[94], P. Loncar[35], X. Lopez[133], E. López Torres[8], P. Luettig[69], J. R. Luhder[143], M. Lunardon[29], G. Luparello[59], M. Lupi[34], A. Maevskaya[62], M. Mager[34], S. M. Mahmood[21], T. Mahmoud[42], A. Maire[135], R. D. Majka[145], M. Malaev[96], Q. W. Malik[21], L. Malinina[75,c], D. Mal'Kevich[64], P. Malzacher[104], A. Mamonov[106], V. Manko[87], F. Manso[133], V. Manzari[52], Y. Mao[6], M. Marchisone[134], J. Mareš[67], G. V. Margagliotti[25], A. Margotti[53], J. Margutti[63], A. Marín[104], C. Markert[118], M. Marquard[69], N. A. Martin[102,104], P. Martinengo[34], J. L. Martinez[125], M. I. Martínez[44], G. Martínez García[113], M. Martinez Pedreira[34], S. Masciocchi[104], M. Masera[26], A. Masoni[54], L. Massacrier[61], E. Masson[113], A. Mastroserio[52,137], A. M. Mathis[103,116], P. F. T. Matuoka[120], A. Matyja[117,129], C. Mayer[117], M. Mazzilli[33], M. A. Mazzoni[57], F. Meddi[23], Y. Melikyan[91], A. Menchaca-Rocha[72], E. Meninno[30], M. Meres[14], S. Mhlanga[124], Y. Miake[132], L. Micheletti[26], M. M. Mieskolainen[43], D. L. Mihaylov[103], K. Mikhaylov[64,75], A. Mischke[63,a], A. N. Mishra[70], D. Miśkowiec[104], C. M. Mitu[68], N. Mohammadi[34], A. P. Mohanty[63], B. Mohanty[85], M. Mohisin Khan[17,d], M. M. Mondal[66], C. Mordasini[103], D. A. Moreira De Godoy[143], L. A. P. Moreno[44], S. Moretto[29], A. Morreale[113], A. Morsch[34], T. Mrnjavac[34], V. Muccifora[51], E. Mudnic[35], D. Mühlheim[143], S. Muhuri[140], M. Mukherjee[3], J. D. Mulligan[79,145], M. G. Munhoz[120], K. Münning[42], R. H. Munzer[69], H. Murakami[131], S. Murray[73], L. Musa[34], J. Musinsky[65], C. J. Myers[125], J. W. Myrcha[141], B. Naik[48], R. Nair[84], B. K. Nandi[48], R. Nania[10,53], E. Nappi[52], M. U. Naru[15], A. F. Nassirpour[80], H. Natal da Luz[120], C. Nattrass[129], S. R. Navarro[44], K. Nayak[85], R. Nayak[48], T. K. Nayak[85,140], S. Nazarenko[106], R. A. Negrao De Oliveira[69], L. Nellen[70], S. V. Nesbo[36], G. Neskovic[39], F. Ng[125], B. S. Nielsen[88], S. Nikolaev[87], S. Nikulin[87], V. Nikulin[96], F. Noferini[10,53], P. Nomokonov[75], G. Nooren[63], J. C. C. Noris[44], J. Norman[78], A. Nyanin[87], J. Nystrand[22], M. Ogino[81], A. Ohlson[102], J. Oleniacz[141], A. C. Oliveira Da Silva[120], M. H. Oliver[145], J. Onderwaater[104], C. Oppedisano[58], R. Orava[43], A. Ortiz Velasquez[70], A. Oskarsson[80], J. Otwinowski[117], K. Oyama[81], Y. Pachmayer[102], V. Pacik[88], D. Pagano[139], G. Paić[70], P. Palni[6], J. Pan[142], A. K. Pandey[48], S. Panebianco[136], V. Papikyan[1], P. Pareek[49], J. Park[60], J. E. Parkkila[126], S. Parmar[98], A. Passfeld[143], S. P. Pathak[125], R. N. Patra[140], B. Paul[58], H. Pei[6], T. Peitzmann[63], X. Peng[6], L. G. Pereira[71], H. Pereira Da Costa[136], D. Peresunko[87], G. M. Perez[8], E. Perez Lezama[69], V. Peskov[69], Y. Pestov[4], V. Petráček[37], M. Petrovici[47], R. P. Pezzi[71], S. Piano[59], M. Pikna[14], P. Pillot[113], L. O. D. L. Pimentel[88], O. Pinazza[34,53], L. Pinsky[125], S. Pisano[51], D. B. Piyarathna[125], M. Płoskoń[79], M. Planinic[97], F. Pliquett[69], J. Pluta[141], S. Pochybova[144], P. L. M. Podesta-Lerma[119], M. G. Poghosyan[94], B. Polichtchouk[90], N. Poljak[97], W. Poonsawat[114], A. Pop[47], H. Poppenborg[143], S. Porteboeuf-Houssais[133], V. Pozdniakov[75], S. K. Prasad[3], R. Preghenella[53], F. Prino[58], C. A. Pruneau[142], I. Pshenichnov[62], M. Puccio[26], V. Punin[106], K. Puranapanda[140], J. Putschke[142], R. E. Quishpe[125], S. Ragoni[108], S. Raha[3], S. Rajput[99], J. Rak[126], A. Rakotozafindrabe[136], L. Ramello[32], F. Rami[135], R. Raniwala[100], S. Raniwala[100], S. S. Räsänen[43], B. T. Rascanu[69], D. Rath[49], V. Ratza[42], I. Ravasenga[31], K. F. Read[94,129], K. Redlich[84,e], A. Rehman[22], P. Reichelt[69], F. Reidt[34], X. Ren[6], R. Renfordt[69], A. Reshetin[62], J.-P. Revol[10], K. Reygers[102], V. Riabov[96], T. Richert[80,88], M. Richter[21], P. Riedler[34], W. Riegler[34], F. Riggi[28], C. Ristea[68], S. P. Rode[49], M. Rodríguez Cahuantzi[44], K. Røed[21], R. Rogalev[90], E. Rogochaya[75], D. Rohr[34], D. Röhrich[22], P. S. Rokita[141], F. Ronchetti[51], E. D. Rosas[70], K. Roslon[141], P. Rosnet[133], A. Rossi[29,56], A. Rotondi[138], F. Roukoutakis[83], A. Roy[49], P. Roy[107], O. V. Rueda[80], R. Rui[25], B. Rumyantsev[75], A. Rustamov[86], E. Ryabinkin[87], Y. Ryabov[96], A. Rybicki[117], S. Saarinen[43], S. Sadhu[140], S. Sadovsky[90], K. Šafařík[34,37], S. K. Saha[140], B. Sahoo[48], P. Sahoo[49], R. Sahoo[49], S. Sahoo[66], P. K. Sahu[66], J. Saini[140], S. Sakai[132], S. Sambyal[99], V. Samsonov[91,96], A. Sandoval[72], A. Sarkar[73], D. Sarkar[140], N. Sarkar[140], P. Sarma[41], V. M. Sarti[103],

M. H. P. Sas[63], E. Scapparone[53], B. Schaefer[94], J. Schambach[118], H. S. Scheid[69], C. Schiaua[47], R. Schicker[102], A. Schmah[102], C. Schmidt[104], H. R. Schmidt[101], M. O. Schmidt[102], M. Schmidt[101], N. V. Schmidt[69,94], A. R. Schmier[129], J. Schukraft[34,88], Y. Schutz[34,135], K. Schwarz[104], K. Schweda[104], G. Scioli[27], E. Scomparin[58], M. Šefčík[38], J. E. Seger[16], Y. Sekiguchi[131], D. Sekihata[45], I. Selyuzhenkov[91,104], S. Senyukov[135], E. Serradilla[72], P. Sett[48], A. Sevcenco[68], A. Shabanov[62], A. Shabetai[113], R. Shahoyan[34], W. Shaikh[107], A. Shangaraev[90], A. Sharma[98], A. Sharma[99], M. Sharma[99], N. Sharma[98], A. I. Sheikh[140], K. Shigaki[45], M. Shimomura[82], S. Shirinkin[64], Q. Shou[6,110], Y. Sibiriak[87], S. Siddhanta[54], T. Siemiarczuk[84], D. Silvermyr[80], G. Simatovic[89], G. Simonetti[34,103], R. Singh[85], R. Singh[99], V. K. Singh[140], V. Singhal[140], T. Sinha[107], B. Sitar[14], M. Sitta[32], T. B. Skaali[21], M. Slupecki[126], N. Smirnov[145], R. J. M. Snellings[63], T. W. Snellman[126], J. Sochan[115], C. Soncco[109], J. Song[60], A. Songmoolnak[114], F. Soramel[29], S. Sorensen[129], F. Sozzi[104], I. Sputowska[117], J. Stachel[102], I. Stan[68], P. Stankus[94], E. Stenlund[80], D. Stocco[113], M. M. Storetvedt[36], P. Strmen[14], A. A. P. Suaide[120], T. Sugitate[45], C. Suire[61], M. Suleymanov[15], M. Suljic[34], R. Sultanov[64], M. Šumbera[93], S. Sumowidagdo[50], K. Suzuki[112], S. Swain[66], A. Szabo[14], I. Szarka[14], U. Tabassam[15], G. Taillepied[133], J. Takahashi[121], G. J. Tambave[22], N. Tanaka[132], S. Tang[6], M. Tarhini[113], M. G. Tarzila[47], A. Tauro[34], G. Tejeda Muñoz[44], A. Telesca[34], C. Terrevoli[29,125], D. Thakur[49], S. Thakur[140], D. Thomas[118], F. Thoresen[88], R. Tieulent[134], A. Tikhonov[62], A. R. Timmins[125], A. Toia[69], N. Topilskaya[62], M. Toppi[51], F. Torales-Acosta[20], S. R. Torres[119], S. Tripathy[49], T. Tripathy[48], S. Trogolo[26], G. Trombetta[33], L. Tropp[38], V. Trubnikov[2], W. H. Trzaska[126], T. P. Trzcinski[141], B. A. Trzeciak[63], T. Tsuji[131], A. Tumkin[106], R. Turrisi[56], T. S. Tveter[21], K. Ullaland[22], E. N. Umaka[125], A. Uras[134], G. L. Usai[24], A. Utrobicic[97], M. Vala[38,115], N. Valle[138], N. van der Kolk[63], L. V. R. van Doremalen[63], J. W. Van Hoorne[34], M. van Leeuwen[63], P. Vande Vyvre[34], D. Varga[144], A. Vargas[44], M. Vargyas[126], R. Varma[48], M. Vasileiou[83], A. Vasiliev[87], O. Vázquez Doce[103,116], V. Vechernin[111], A. M. Veen[63], E. Vercellin[26], S. Vergara Limón[44], L. Vermunt[63], R. Vernet[7], R. Vértesi[144], L. Vickovic[35], J. Viinikainen[126], Z. Vilakazi[130], O. Villalobos Baillie[108], A. Villatoro Tello[44], G. Vino[52], A. Vinogradov[87], T. Virgili[30], V. Vislavicius[88], A. Vodopyanov[75], B. Volkel[34], M. A. Völkl[101], K. Voloshin[64], S. A. Voloshin[142], G. Volpe[33], B. von Haller[34], I. Vorobyev[103,116], D. Voscek[115], J. Vrláková[38], B. Wagner[22], M. Wang[6], Y. Watanabe[132], M. Weber[112], S. G. Weber[104], A. Wegrzynek[34], D. F. Weiser[102], S. C. Wenzel[34], J. P. Wessels[143], U. Westerhoff[143], A. M. Whitehead[124], E. Widmann[112], J. Wiechula[69], J. Wikne[21], G. Wilk[84], J. Wilkinson[53], G. A. Willems[34,143], E. Willsher[108], B. Windelband[102], W. E. Witt[129], Y. Wu[128], R. Xu[6], S. Yalcin[77], K. Yamakawa[45], S. Yang[22], S. Yano[136], Z. Yin[6], H. Yokoyama[63], I.-K. Yoo[18], J. H. Yoon[60], S. Yuan[22], V. Yurchenko[2], V. Zaccolo[25,58], A. Zaman[15], C. Zampolli[34], H. J. C. Zanoli[120], N. Zardoshti[34,108], A. Zarochentsev[111], P. Závada[67], N. Zaviyalov[106], H. Zbroszczyk[141], M. Zhalov[96], X. Zhang[6], Y. Zhang[6], Z. Zhang[6,133], C. Zhao[21], V. Zherebchevskii[111], N. Zhigareva[64], D. Zhou[6], Y. Zhou[88], Z. Zhou[22], H. Zhu[6], J. Zhu[6], Y. Zhu[6], A. Zichichi[10,27], M. B. Zimmermann[34], G. Zinovjev[2], N. Zurlo[139]

[1] A.I. Alikhanyan National Science Laboratory (Yerevan Physics Institute) Foundation, Yerevan, Armenia
[2] Bogolyubov Institute for Theoretical Physics, National Academy of Sciences of Ukraine, Kiev, Ukraine
[3] Department of Physics, Bose Institute, Centre for Astroparticle Physics and Space Science (CAPSS), Kolkata, India
[4] Budker Institute for Nuclear Physics, Novosibirsk, Russia
[5] California Polytechnic State University, San Luis Obispo, CA, USA
[6] Central China Normal University, Wuhan, China
[7] Centre de Calcul de l'IN2P3, Villeurbanne, Lyon, France
[8] Centro de Aplicaciones Tecnológicas y Desarrollo Nuclear (CEADEN), Havana, Cuba
[9] Centro de Investigación y de Estudios Avanzados (CINVESTAV), Mexico, Mérida, Mexico
[10] Centro Fermi-Museo Storico della Fisica e Centro Studi e Ricerche "Enrico Fermi', Rome, Italy
[11] Chicago State University, Chicago, IL, USA
[12] China Institute of Atomic Energy, Beijing, China
[13] Chonbuk National University, Jeonju, Republic of Korea
[14] Faculty of Mathematics, Physics and Informatics, Comenius University Bratislava, Bratislava, Slovakia
[15] COMSATS University Islamabad, Islamabad, Pakistan
[16] Creighton University, Omaha, NE, USA
[17] Department of Physics, Aligarh Muslim University, Aligarh, India
[18] Department of Physics, Pusan National University, Pusan, Republic of Korea
[19] Department of Physics, Sejong University, Seoul, Republic of Korea
[20] Department of Physics, University of California, Berkeley, CA, USA
[21] Department of Physics, University of Oslo, Oslo, Norway
[22] Department of Physics and Technology, University of Bergen, Bergen, Norway

[23] Dipartimento di Fisica dell'Università 'La Sapienza' and Sezione INFN, Rome, Italy

[24] Dipartimento di Fisica dell'Università and Sezione INFN, Cagliari, Italy

[25] Dipartimento di Fisica dell'Università and Sezione INFN, Trieste, Italy

[26] Dipartimento di Fisica dell'Università and Sezione INFN, Turin, Italy

[27] Dipartimento di Fisica e Astronomia dell'Università and Sezione INFN, Bologna, Italy

[28] Dipartimento di Fisica e Astronomia dell'Università and Sezione INFN, Catania, Italy

[29] Dipartimento di Fisica e Astronomia dell'Università and Sezione INFN, Padua, Italy

[30] Dipartimento di Fisica 'E.R. Caianiello' dell'Università and Gruppo Collegato INFN, Salerno, Italy

[31] Dipartimento DISAT del Politecnico and Sezione INFN, Turin, Italy

[32] Dipartimento di Scienze e Innovazione Tecnologica dell'Università del Piemonte Orientale and INFN Sezione di Torino, Alessandria, Italy

[33] Dipartimento Interateneo di Fisica 'M. Merlin' and Sezione INFN, Bari, Italy

[34] European Organization for Nuclear Research (CERN), Geneva, Switzerland

[35] Faculty of Electrical Engineering, Mechanical Engineering and Naval Architecture, University of Split, Split, Croatia

[36] Faculty of Engineering and Science, Western Norway University of Applied Sciences, Bergen, Norway

[37] Faculty of Nuclear Sciences and Physical Engineering, Czech Technical University in Prague, Prague, Czech Republic

[38] Faculty of Science, P.J. Šafárik University, Kosice, Slovakia

[39] Frankfurt Institute for Advanced Studies, Johann Wolfgang Goethe-Universität Frankfurt, Frankfurt, Germany

[40] Gangneung-Wonju National University, Gangneung, Republic of Korea

[41] Department of Physics, Gauhati University, Guwahati, India

[42] Helmholtz-Institut für Strahlen- und Kernphysik, Rheinische Friedrich-Wilhelms-Universität Bonn, Bonn, Germany

[43] Helsinki Institute of Physics (HIP), Helsinki, Finland

[44] High Energy Physics Group, Universidad Autónoma de Puebla, Puebla, Mexico

[45] Hiroshima University, Hiroshima, Japan

[46] Hochschule Worms, Zentrum für Technologietransfer und Telekommunikation (ZTT), Worms, Germany

[47] Horia Hulubei National Institute of Physics and Nuclear Engineering, Bucharest, Romania

[48] Indian Institute of Technology Bombay (IIT), Mumbai, India

[49] Indian Institute of Technology Indore, Indore, India

[50] Indonesian Institute of Sciences, Jakarta, Indonesia

[51] INFN, Laboratori Nazionali di Frascati, Frascati, Italy

[52] INFN, Sezione di Bari, Bari, Italy

[53] INFN, Sezione di Bologna, Bologna, Italy

[54] INFN, Sezione di Cagliari, Cagliari, Italy

[55] INFN, Sezione di Catania, Catania, Italy

[56] INFN, Sezione di Padova, Padua, Italy

[57] INFN, Sezione di Roma, Rome, Italy

[58] INFN, Sezione di Torino, Turin, Italy

[59] INFN, Sezione di Trieste, Trieste, Italy

[60] Inha University, Inchon, Republic of Korea

[61] Institut de Physique Nucléaire d'Orsay (IPNO), Institut National de Physique Nucléaire et de Physique des Particules (IN2P3/CNRS), Université de Paris-Sud, Université Paris-Saclay, Orsay, France

[62] Institute for Nuclear Research, Academy of Sciences, Moscow, Russia

[63] Institute for Subatomic Physics, Utrecht University/Nikhef, Utrecht, Netherlands

[64] Institute for Theoretical and Experimental Physics, Moscow, Russia

[65] Institute of Experimental Physics, Slovak Academy of Sciences, Košice, Slovakia

[66] Institute of Physics, Homi Bhabha National Institute, Bhubaneswar, India

[67] Institute of Physics of the Czech Academy of Sciences, Prague, Czech Republic

[68] Institute of Space Science (ISS), Bucharest, Romania

[69] Institut für Kernphysik, Johann Wolfgang Goethe-Universität Frankfurt, Frankfurt, Germany

[70] Instituto de Ciencias Nucleares, Universidad Nacional Autónoma de México, Mexico City, Mexico

[71] Instituto de Física, Universidade Federal do Rio Grande do Sul (UFRGS), Porto Alegre, Brazil

[72] Instituto de Física, Universidad Nacional Autónoma de México, Mexico City, Mexico

[73] iThemba LABS, National Research Foundation, Somerset West, South Africa

[74] Johann-Wolfgang-Goethe Universität Frankfurt Institut für Informatik, Fachbereich Informatik und Mathematik, Frankfurt, Germany

[75] Joint Institute for Nuclear Research (JINR), Dubna, Russia

[76] Korea Institute of Science and Technology Information, Taejon, Republic of Korea

[77] KTO Karatay University, Konya, Turkey

[78] Laboratoire de Physique Subatomique et de Cosmologie, Université Grenoble-Alpes, CNRS-IN2P3, Grenoble, France

[79] Lawrence Berkeley National Laboratory, Berkeley, CA, USA

[80] Division of Particle Physics, Department of Physics, Lund University, Lund, Sweden

[81] Nagasaki Institute of Applied Science, Nagasaki, Japan

[82] Nara Women's University (NWU), Nara, Japan

[83] School of Science, Department of Physics, National and Kapodistrian University of Athens, Athens, Greece

[84] National Centre for Nuclear Research, Warsaw, Poland

[85] National Institute of Science Education and Research, Homi Bhabha National Institute, Jatni, India

[86] National Nuclear Research Center, Baku, Azerbaijan

[87] National Research Centre Kurchatov Institute, Moscow, Russia

[88] Niels Bohr Institute, University of Copenhagen, Copenhagen, Denmark

[89] Nikhef, National institute for subatomic physics, Amsterdam, The Netherlands

[90] NRC Kurchatov Institute IHEP, Protvino, Russia

[91] NRNU Moscow Engineering Physics Institute, Moscow, Russia

[92] Nuclear Physics Group, STFC Daresbury Laboratory, Daresbury, UK

[93] Nuclear Physics Institute of the Czech Academy of Sciences, Řež u Prahy, Czech Republic

[94] Oak Ridge National Laboratory, Oak Ridge, TN, USA

[95] Ohio State University, Columbus, Ohio, USA

[96] Petersburg Nuclear Physics Institute, Gatchina, Russia

[97] Physics Department, Faculty of science, University of Zagreb, Zagreb, Croatia

[98] Physics Department, Panjab University, Chandigarh, India

[99] Physics Department, University of Jammu, Jammu, India

[100] Physics Department, University of Rajasthan, Jaipur, India

[101] Physikalisches Institut, Eberhard-Karls-Universität Tübingen, Tübingen, Germany

[102] Physikalisches Institut, Ruprecht-Karls-Universität Heidelberg, Heidelberg, Germany

[103] Physik Department, Technische Universität München, Munich, Germany

[104] Research Division and ExtreMe Matter Institute EMMI, GSI Helmholtzzentrum für Schwerionenforschung GmbH, Darmstadt, Germany

[105] Rudjer Bošković Institute, Zagreb, Croatia

[106] Russian Federal Nuclear Center (VNIIEF), Sarov, Russia

[107] Saha Institute of Nuclear Physics, Homi Bhabha National Institute, Kolkata, India

[108] School of Physics and Astronomy, University of Birmingham, Birmingham, UK

[109] Sección Física, Departamento de Ciencias, Pontificia Universidad Católica del Perú, Lima, Peru

[110] Shanghai Institute of Applied Physics, Shanghai, China

[111] St. Petersburg State University, St. Petersburg, Russia

[112] Stefan Meyer Institut für Subatomare Physik (SMI), Vienna, Austria

[113] SUBATECH, IMT Atlantique, Université de Nantes, CNRS-IN2P3, Nantes, France

[114] Suranaree University of Technology, Nakhon Ratchasima, Thailand

[115] Technical University of Košice, Kosice, Slovakia

[116] Technische Universität München, Excellence Cluster 'Universe', Munich, Germany

[117] The Henryk Niewodniczanski Institute of Nuclear Physics, Polish Academy of Sciences, Kraków, Poland

[118] The University of Texas at Austin, Austin, TX, USA

[119] Universidad Autónoma de Sinaloa, Culiacán, Mexico

[120] Universidade de São Paulo (USP), São Paulo, Brazil

[121] Universidade Estadual de Campinas (UNICAMP), Campinas, Brazil

[122] Universidade Federal do ABC, Santo Andre, Brazil

[123] University College of Southeast Norway, Tonsberg, Norway

[124] University of Cape Town, Cape Town, South Africa

[125] University of Houston, Houston, Texas, USA

[126] University of Jyväskylä, Jyväskylä, Finland

[127] University of Liverpool, Liverpool, UK

[128] University of Science and Techonology of China, Hefei, China

[129] University of Tennessee, Knoxville, TN, USA

[130] University of the Witwatersrand, Johannesburg, South Africa

[131] University of Tokyo, Tokyo, Japan

[132] University of Tsukuba, Tsukuba, Japan

[133] Université Clermont Auvergne, CNRS/IN2P3, LPC, Clermont-Ferrand, France

[134] Université de Lyon, Université Lyon 1, CNRS/IN2P3, IPN-Lyon, Villeurbanne, Lyon, France

[135] Université de Strasbourg, CNRS, IPHC UMR 7178, 67000 Strasbourg, France

[136] Department de Physique Nucléaire (DPhN), Université Paris-Saclay Centre dÉtudes de Saclay (CEA), IRFU, Saclay, France

[137] Università degli Studi di Foggia, Foggia, Italy

[138] Università degli Studi di Pavia, Pavia, Italy

[139] Università di Brescia, Brescia, Italy

[140] Variable Energy Cyclotron Centre, Homi Bhabha National Institute, Kolkata, India

[141] Warsaw University of Technology, Warsaw, Poland

[142] Wayne State University, Detroit, MI, USA

[143] Westfälische Wilhelms-Universität Münster, Institut für Kernphysik, Münster, Germany

[144] Wigner Research Centre for Physics, Hungarian Academy of Sciences, Budapest, Hungary

[145] Yale University, New Haven, CT, USA

[146] Yonsei University, Seoul, Republic of Korea

[a] Deceased

[b] Dipartimento DET del Politecnico di Torino, Turin, Italy

[c] M.V. Lomonosov Moscow State University, D.V. Skobeltsyn Institute of Nuclear, Physics, Moscow, Russia

[d] Department of Applied Physics, Aligarh Muslim University, Aligarh, India

[e] Institute of Theoretical Physics, University of Wroclaw, Poland